This is a repository copy of *Multi-objective Optimization of Zero Propellant Spacecraft Attitude Maneuvers*.

White Rose Research Online URL for this paper:
http://eprints.whiterose.ac.uk/81034/

Version: Accepted Version

Article:

Zhang, S., Tang, G.J., Friswell, M.I. et al. (1 more author) (2014) Multi-objective Optimization of Zero Propellant Spacecraft Attitude Maneuvers. Journal of Optimization Theory and Applications. 1 - 23. ISSN 0022-3239

https://doi.org/10.1007/s10957-014-0524-8

Reuse

Unless indicated otherwise, fulltext items are protected by copyright with all rights reserved. The copyright exception in section 29 of the Copyright, Designs and Patents Act 1988 allows the making of a single copy solely for the purpose of non-commercial research or private study within the limits of fair dealing. The publisher or other rights-holder may allow further reproduction and re-use of this version - refer to the White Rose Research Online record for this item. Where records identify the publisher as the copyright holder, users can verify any specific terms of use on the publisher's website.

Takedown

If you consider content in White Rose Research Online to be in breach of UK law, please notify us by emailing eprints@whiterose.ac.uk including the URL of the record and the reason for the withdrawal request.

eprints@whiterose.ac.uk
https://eprints.whiterose.ac.uk/

Manuscript
Click here to download Manuscript: 1.Manuscript.doc
Click here to view linked References

Multi-objective Optimization of Zero Propellant Spacecraft Attitude Maneuvers*

S. Zhang[1] • G.J. Tang[2] • M.I Friswell[3] • D.J Wagg[4]

Communicated by Mauro Pontani

Abstract The zero propellant maneuver is an advanced space station, large angle attitude maneuver technique, using only control momentum gyroscopes. Path planning is the key to success and this paper studies the associated multi-objective optimization problem. Three types of maneuver optimal control problem are formulated: (i) momentum-optimal, (ii) time-optimal and, (iii) energy-optimal. A sensitivity analysis approach is used to study the Pareto optimal front and allows the tradeoffs between the performance indices to be investigated. For example, it is proved that the minimum peak momentum decreases as the maneuver time increases, and the minimum maneuver energy decreases if a larger momentum is available from the control momentum gyroscopes. The analysis is verified and complemented by the numerical computations. Among the three types of zero propellant maneuver paths, the momentum-optimal solution and the time-optimal solution generally possess the same structure, and they are singular. The energy-optimal solution saves significant energy, while generally maintaining a smooth control profile.

AMS Classification 90C29

Keywords Space station • Zero Propellant Maneuver (ZPM) • Multi-objective Optimization Problem (MOP) • Pareto optimal front • Sensitivity analysis

---

* Research supported by the National Natural Science Foundation of China, grant number: 11272346.

1 *College of Aerospace Science and Engineering, National University of Defense Technology, Changsha, China. 410073*. Email: zszhangshengzs@hotmail.com

2 *College of Aerospace Science and Engineering, National University of Defense Technology, Changsha, China. 410073*. **Corresponding author**, Email: tang_guojin@hotmail.com.

3 *College of Engineering, Swansea University, Singleton Park, Swansea SA2 8PP, UK*.

4 *Faculty of Engineering, University of Bristol, University Walk, Bristol BS8 1TR, UK*.

1 Introduction

NASA has successfully conducted two Zero Propellant Maneuver (ZPM) missions on 5 November 2006 and 3 March 2007, when the International Space Station (ISS) was rotated by 90° [1] and 180° [2], respectively. The ZPM technique is a new concept to maneuver a space station using only Control Momentum Gyroscopes (CMGs). In particular, the environmental torque is exploited to enable large angle maneuvers to be achieved, whilst simultaneously maintaining the CMGs within their operational limit [3]. A ZPM is a complex attitude maneuver guidance problem, in which maneuver path planning is the key to success. The executed trajectories of the two ZPM missions were momentum-optimal. The momentum objective, defined in the Optimal Control Problem (OCP), gives the maneuver path with the largest CMGs angular momentum redundancy, which brings increased robustness to the angular momentum deviations arising from various disturbances [4]. This robustness is especially important for paths that are planned off-line. However, the momentum-optimal path has a large rate of momentum change of the CMGs around the initial and final times that require fast gimbal motion, which may harm the CMGs. Thus, maneuver path types, other than momentum-optimal, should be studied, and different path types synthesized. The other types of maneuver paths require different objectives in the ZPM OCP formulation; typical examples include the energy-optimal and the time-optimal paths. The optimal energy performance index yields the maneuver path, which minimizes the energy consumed. Since the electrical power that dives the CMGs is limited on-board, methods to save energy have practical value. The optimal time performance index seeks the path that gives the minimum time to fulfill the maneuver and this improved agility is required under certain situations.

The momentum-optimal solution is specific to the ZPM OCP. Although energy- or time-optimal attitude maneuver problems have been studied for decades, the ZPM OCP version differs in a number of respects that are now outlined. First, in a ZPM the motion of the CMGs needs to be considered and, generally, the angular momentum of the CMGs has a final state requirement. Second, generally the ZPM is a rest-to-rest reorientation with respect to the orbit reference frame instead of the inertial frame, and thus the rotation of the orbit frame needs to be considered. Third, the path constraint of the ZPM is not a simple bounded control torque constraint, but is more complex since the angular momentum and the rate of momentum change of the CMGs must be restricted within their allowable range. Fourth, the environmental torque must be exploited to realize a ZPM, while it is neglected in the classic optimal attitude maneuver studies. The total angular momentum of the spacecraft system, including the space station body and the CMGs, may change greatly during a ZPM. As an angular momentum change device, the CMGs cannot produce the angular momentum. Thus, the environmental torque is required to realize the momentum change for the

ZPM. These differences show the inapplicability of classic OCP results and highlight the necessity to study the ZPM problem.

The three performance indices may be considered as a Multi-objective Optimization Problem (MOP). In general, a solution, which optimizes all of the performance indices simultaneously, does not exist, and a compromise solution has to be sought. The concept of the Pareto optimum is a widely accepted tradeoff between the objectives [5]. Generally, the Pareto optimal set of the MOP must be determined numerically. There are two types of numerical methods; either the MOP is transformed to a set of Single-objective Optimization Problems (SOP) to be solved, or an evolutionary algorithm is utilized to solve the MOP directly [5]. Often large amount of computation is required to obtain the optimal front for a complex MOP, particularly to ensure that the numerical results uncover the tradeoff relationship with adequate accuracy. In an optimization problem, if the optimized performance index is a function of a parameter, which may be another performance index, then the Pareto optimal front may be investigated using the derivative, i.e. the sensitivity. For example, for a minimization MOP with two objectives, the first order sensitivity of the optimal front curve is negative and strictly monotonic. Thus the sensitivity analysis may be used to gain insight into the Pareto optimal front. To verify and complement the resulting conclusions, numerical computations are also performed using GPOPS (version 5.2) [6], which employs the Radau Pseudo Spectral (PS) method [7].

The paper is organized as follows. The ZPM MOP is formulated in Section 2. Section 3 presents the sensitivity analysis theory of the OCP objective with respect to a parameter. In Section 4, the ZPM MOP is studied, the optimal solutions for a single objective are investigated, and the conclusions, deduced using the sensitivity analysis method, are verified and complemented by the numerical computations.

2 Formulation of the ZPM MOP

2.1 State Equations

To derive the equations of motion, relevant reference frames are defined first. The body reference frame, *b*, has its origin at the center of mass of the space station. It is fixed with the space station and its axes are aligned with the geometric characteristic directions, which are not necessarily the principal inertia axes. The Local Vertical Local Horizontal (LVLH) orbit reference frame, o, has origin o_o that coincides with the center of mass of the space station. The $o_o z_o$ axis is aligned with the local vertical, towards the centre of Earth, the $o_o x_o$ axis lies on the orbit plane in the transverse direction, normal to $o_o z_o$, and the $o_o y_o$ axis is perpendicular to the orbit plane, completing a right-handed triad. The orbit frame makes one rotation about the Earth during each orbit period. In this paper, a circular orbit is assumed for the space station, so that the orbit rotation rate, n, is constant.

The Modified Rodrigues Parameters (MRPs) are the minimal description of attitude, which avoids singularities for a principal rotation up to ± 360 deg [8]. They are defined as

$$\boldsymbol{\sigma} := \begin{bmatrix} \sigma_1 & \sigma_2 & \sigma_3 \end{bmatrix}^{\mathrm{T}} := \boldsymbol{e} \tan \frac{\theta}{4}, \tag{1}$$

where $\boldsymbol{e}$ is the principal rotation axis and θ is the principal rotation angle. The kinematic equation which describes the attitude of the space station with respect to the orbit is

$$\dot{\boldsymbol{\sigma}} = \boldsymbol{T}(\boldsymbol{\sigma})\left(\boldsymbol{\omega} - \boldsymbol{\omega}_o\right), \tag{2}$$

where $\boldsymbol{T}(\boldsymbol{\sigma})$ is the kinematic matrix, $\boldsymbol{\omega}$ and $\boldsymbol{\omega}_o = \boldsymbol{R}_o^b(\boldsymbol{\sigma})\begin{bmatrix} 0 & -n & 0 \end{bmatrix}^{\mathrm{T}}$ are the space station angular velocity and the orbit frame angular velocity, described in the body frame, respectively, $\boldsymbol{R}_o^b$ is the rotation matrix from the orbit frame, o, to the body frame, b. The specific form of $\boldsymbol{T}(\boldsymbol{\sigma})$ and $\boldsymbol{R}_o^b$ are given by Schaub *et al*. [8].

The dynamic equation described in the body reference frame is

$$\dot{\boldsymbol{\omega}} = \boldsymbol{J}^{-1}\left(\boldsymbol{\tau}_{\mathrm{e}} - \boldsymbol{u} - \boldsymbol{\omega} \times (\boldsymbol{J}\boldsymbol{\omega})\right), \tag{3}$$

where $\boldsymbol{J}$ is the inertia matrix of the space station, $\boldsymbol{u}$ is the control generated by the CMGs, and the "×" denotes the vector cross product. The environmental torques acting on the space station, $\boldsymbol{\tau}_{\mathrm{e}}$, include the earth gravity gradient torque, the aerodynamic torque and other types of torques. Since the magnitude of the other environmental torques is much smaller than that of the gravity gradient torque and the aerodynamic torque, they are neglected in the path planning problem. The models for the gravity gradient torque and the aerodynamic torque are given by Bhatt [4].

The motion of the CMGs must also be considered in the maneuver, because of their limited capacity and the boundary condition constraints. The equation of motion of the CMGs is

$$\dot{\boldsymbol{h}}_{\mathrm{cmg}} = \boldsymbol{u} - \boldsymbol{\omega} \times \boldsymbol{h}_{\mathrm{cmg}}, \tag{4}$$

where $\boldsymbol{h}_{\mathrm{cmg}}$ is the angular momentum of the CMGs described in the body frame. In order to apply the analysis theory developed in next section, here the pseudo-control $\boldsymbol{w}$ is defined as

$$\boldsymbol{w} := \boldsymbol{u} - \boldsymbol{\omega} \times \boldsymbol{h}_{\mathrm{cmg}}. \tag{5}$$

The transformation of the control does not affect the solution of the OCP, but it guarantees the rigorousness of the sensitivity analysis. Equations (3) and (4) are transformed to

$$\dot{\boldsymbol{\omega}} = \boldsymbol{J}^{-1}\left(\boldsymbol{\tau}_{\mathrm{e}} - \boldsymbol{w} - \boldsymbol{\omega} \times (\boldsymbol{J}\boldsymbol{\omega} + \boldsymbol{h}_{\mathrm{cmg}})\right), \tag{6}$$

$$\dot{\boldsymbol{h}}_{\mathrm{cmg}} = \boldsymbol{w}. \tag{7}$$

2.2 Boundary Conditions

Generally, a ZPM transfers the space station from one Torque Equilibrium Attitude (TEA) to another. For a TEA, the attitude and corresponding angular velocity are associated, and the CMGs momentum state is prescribed for the momentum management [4]. The general form of the initial and final boundary conditions is

$$\boldsymbol{\sigma}(t_0) = \boldsymbol{\sigma}_0, \quad \boldsymbol{\omega}(t_0) = \boldsymbol{\omega}_0, \quad \boldsymbol{h}_{\mathrm{cmg}}(t_0) = \boldsymbol{h}_0, \tag{8}$$

$$\boldsymbol{\sigma}(t_f) = \boldsymbol{\sigma}_f, \quad \boldsymbol{\omega}(t_f) = \boldsymbol{\omega}_f, \quad \boldsymbol{h}_{\mathrm{cmg}}(t_f) = \boldsymbol{h}_f, \tag{9}$$

where t_0 is the initial time, and t_f is the final time. In this paper, the initial time t_0 is set to be zero, so that t_f represents the maneuver time. $\boldsymbol{\sigma}_0$, $\boldsymbol{\omega}_0$, $\boldsymbol{h}_0$ and $\boldsymbol{\sigma}_f$, $\boldsymbol{\omega}_f$, $\boldsymbol{h}_f$ are the prescribed initial and final boundary conditions, respectively.

2.3 Path Constraints

CMGs have limits on their angular momentum and torque. Hence, during a maneuver the CMGs must operate within their performance range, which may be written as constraints on the angular momentum and the rate of angular momentum change [4] as

$$\left\| \boldsymbol{h}_{\mathrm{cmg}} \right\|^2 \le h_{\max}^2, \tag{10}$$

and

$$\left\| \frac{\mathrm{d}\boldsymbol{h}_{\mathrm{cmg}}}{\mathrm{d}t} \right\|^2 \le \dot{h}_{\max}^2, \tag{11}$$

where $h_{\max}$ and $\dot{h}_{\max}$ are the momentum magnitude parameter and the rate of momentum change magnitude parameter, respectively. Note that the path constraints involve the Euclidean norm squared to ensure they are differentiable at zero. The first constraint is called the momentum constraint, which is a state constraint. The second constraint is called the rate of momentum change constraint. Using the control transformation given by (5), it may be transformed to a pure control constraint from a mixed state-control constraint.

2.4 Objectives

Three objectives are considered for the ZPM, namely the momentum objective, the time objective and the energy objective. The momentum objective represents the peak angular momentum of the CMGs during the maneuver, and takes the form

$$J_1 := \gamma, \qquad \text{where} \quad \gamma := h_{\max}^2. \tag{12}$$

This objective is equivalent to a Mayer objective $\gamma(t_f)$, which may be induced by regarding γ as a state variable with state equation, $\dot{\gamma}=0$. The momentum-optimal control problem seeks the solution with minimum peak momentum during the maneuver, i.e. $r := \min \gamma$.

The time objective is the maneuver time. Thus

$$J_2 := t_f . \tag{13}$$

The maneuver time in the time-optimal control problem is denoted as $\tau := \min t_f$.

The energy consumed during the maneuver is an important measure of the control performance. In the paper the energy is represented by the integral of the square control torque, which is related to the energy consumed. Thus, the performance index is

$$E := \int_{t_0}^{t_f} \boldsymbol{u}^{\mathrm{T}} \boldsymbol{u} \, \mathrm{d}t = \int_{t_0}^{t_f} (\boldsymbol{w} + \boldsymbol{\omega} \times \boldsymbol{h}_{\mathrm{cmg}})^{\mathrm{T}} (\boldsymbol{w} + \boldsymbol{\omega} \times \boldsymbol{h}_{\mathrm{cmg}}) \, \mathrm{d}t , \tag{14}$$

and the energy objective is

$$J_3 := E . \tag{15}$$

The energy performance in the energy-optimal control problem is denoted as $e := \min E$, which has units of $\mathrm{N^2m^2s}$ rather than energy.

The ZPM MOP is now defined. The objectives are given by (12), (13) and (15), the state equations are given by (2), (6) and (7), the boundary conditions are given by (8) and (9), and the path constraints are given by (10) and (11).

3 Sensitivity Analysis

Consider a parameter in the optimization problem. Then the optimal performance index is a function of that parameter, and the analytical form of this function is often impossible to obtain explicitly. An alternative is to study the derivative, i.e. the sensitivity, of the function to the parameter about a baseline value. The first order sensitivity represents the tangent slope and the second order sensitivity represents the convexity. Generally, the sign of these two sensitivities determines the basic shape of the function, thus uncovering the influence of parameter changes on the optimal value. If the parameter is the value of one of the performance indices, then the sensitivity gives information on the Pareto optimal front.

Rehbock *et al*. [9] calculated the first order sensitivity of the optimal performance index with respect to a static parameter, but the result is limited to the unconstrained OCP with free final states. In this section, the sensitivity with respect to static parameters is generalized to the constrained OCP. Because the final time t_f is often an important parameter as well as a performance index, the sensitivity to t_f is also presented. For the subsequent studies, an initial assumption is that, if a solution to the OCP exits, then it is continuously differentiable with respect to the perturbation parameter of interest [10].

Lemma 3.1 The constrained optimal control problem is given by

$$K := \min\left(J\right), \tag{16}$$

subject to

$$\begin{gathered} \dot{\boldsymbol{x}} = \boldsymbol{f}(\boldsymbol{x},\boldsymbol{u},t;a), \\ \boldsymbol{\varphi}(\boldsymbol{x}(t_0),t_0;a) = \boldsymbol{0}, \qquad \boldsymbol{\psi}(\boldsymbol{x}(t_f),t_f;a) = \boldsymbol{0}, \\ \boldsymbol{C}(\boldsymbol{x},\boldsymbol{u},t;a) \le \boldsymbol{0}, \qquad \boldsymbol{S}(\boldsymbol{x},t;a) \le \boldsymbol{0}, \end{gathered}$$

where $J := \phi(\boldsymbol{x}(t_f),t_f;a) + \int_{t_0}^{t_f} L(\boldsymbol{x},\boldsymbol{u},t;a)\mathrm{d}t$, $\boldsymbol{x}$ is the n dimensional state variable vector, $\boldsymbol{u}$ is the m dimensional control variable vector, a is the static parameter, and the final time t_f may be fixed or free. In (16), $\dot{\boldsymbol{x}} = \boldsymbol{f}$ is the state equation, and $\boldsymbol{\varphi}$ and $\boldsymbol{\psi}$ are the initial and final boundary conditions, respectively. $\boldsymbol{C}$ and $\boldsymbol{S}$ are path constraints, and represent the mixed state-control inequality constraint and the state inequality constraint respectively. Then, the sensitivity to the static parameter is calculated as

$$\frac{\mathrm{d}K}{\mathrm{d}a} = \boldsymbol{\pi}_0 \cdot \boldsymbol{\varphi}_a + \boldsymbol{\pi}_f \cdot \boldsymbol{\psi}_a + \phi_a + \int_{t_0}^{t_f} (\bar{H}_a)\mathrm{d}t, \tag{17}$$

where $\bar{H} := L + \boldsymbol{\lambda} \cdot \boldsymbol{f} + \boldsymbol{v} \cdot \boldsymbol{S} + \boldsymbol{\mu} \cdot \boldsymbol{C}$ is the augmented Hamiltonian, $\boldsymbol{\pi}_0$ and $\boldsymbol{\pi}_f$ are the Lagrange multiplier parameters, $\boldsymbol{\lambda}$ is the costate vector, $\boldsymbol{v}$ and $\boldsymbol{\mu}$ are the Karush-Kuhn-Tucker (KKT) multiplier variables, and the "$\cdot$" denotes the vector dot product. The subscript a denotes the partial derivative with respect to a, for example $\boldsymbol{\varphi}_a = \dfrac{\partial \boldsymbol{\varphi}}{\partial a}$.

Lemma 3.1 may be proved by investigating the variation of the objective functional with respect to the variation of the parameter along the optimal solution. Thus, (17) is obtained from

$$\frac{\mathrm{d}}{\mathrm{d}a}\left(\min\left(\bar{J}(\boldsymbol{x},\boldsymbol{u},t;a)\right)\right) = \frac{\partial}{\partial a}\left(\bar{J}(\boldsymbol{x},\boldsymbol{u},t;a)\right)\bigg|_{\boldsymbol{x}^*,\boldsymbol{u}^*}, \tag{18}$$

where $\bar{J} := \boldsymbol{\pi}_0 \cdot \boldsymbol{\varphi} + \pi_f \cdot \boldsymbol{\psi} + \phi + \int_{t_0}^{t_f} (L + \boldsymbol{\lambda} \cdot (\boldsymbol{f} - \dot{\boldsymbol{x}}) + \boldsymbol{v} \cdot \boldsymbol{S} + \boldsymbol{\mu} \cdot \boldsymbol{C})\mathrm{d}t$ is the augmented objective obtained through the direct adjoining method [11], and $\boldsymbol{x}^*$ and $\boldsymbol{u}^*$ denote the optimal solutions corresponding to a specified parameter a. Note that the sensitivity given by Rehbock *et al*. [9] is a special case of (17).

Lemma 3.2 For the constrained optimal control problem given by (16) with fixed final time t_f,

$$\frac{\mathrm{d}K}{\mathrm{d}t_f} = \boldsymbol{\pi}_f \cdot \boldsymbol{\psi}_{t_f} + \phi_{t_f} + H(t_f), \tag{19}$$

where $H := L + \boldsymbol{\lambda} \cdot \boldsymbol{f}$ is the Hamiltonian.

Lemma 3.2 is proved in the same way as Lemma 3.1. Equation (19) is consistent with the first order optimality condition when the final time is free. When the sensitivity is zero, i.e. $\frac{\mathrm{d}K}{\mathrm{d}t_f} = 0$, the optimal condition with respect to the final time variation is obtained.

It will be shown that, by utilizing the property of the boundary conditions or KKT multiplier, the signs of the first order sensitivities presented in the Lemmas may be determined without solving the OCP, thus presenting qualitative results. The treatment in the presence of state inequality constraints is complex. When there are both state inequality constraints and mixed state-control inequality constraints, the applicability of the direct adjoining method is not fully proved. In [11], several specific cases are listed. When the mixed state-control inequality constraint is independent of the state, reducing to a pure control inequality constraint, the applicability is proven. The reason why the pseudo-control is defined in (5) is to guarantee the applicability of the theory developed here.

4 Study of the ZPM MOP

In this section, the optimal solutions for single objectives are investigated first. Then, the three objectives are considered in pairs to understand the tradeoffs between the objectives. Finally, the results are synthesized to gain insight into the potential solutions. To verify and complement the analytical results obtained, a common example taken from [4] will be used. The maneuver is an approximate −90 deg rotation from a +XVV TEA to +YVV TEA. The orbital rotation rate is $n = 1.1461\times10^{-3}$ rad/s, and the inertia matrix of the space station is

$$\boldsymbol{J} = \begin{bmatrix} 24180443 & 3780009 & 3896127 \\ 3780010 & 37607882 & -1171169 \\ 3896127 & -1171169 & 51562389 \end{bmatrix} \mathrm{kg\ m^2}.$$

The constraints for the CMGs are a maximum momentum of $h_{\max} = 1.9524\times10^4$ N m s and a maximum rate of change of momentum of $\dot{h}_{\max} = 271.16$ N m. The aerodynamic model utilizes a mass density of the atmosphere of 2×10^{-11} kg/m^3, and the drag coefficient is 2.2. The space station body includes two parts: the center body and the solar arrays. The center body is modeled by a quasi-cylinder of length 45 m and radius 2.25 m. The solar arrays are represented by two symmetrical plates of length 20 m and width 4 m. Described in the body frame, The vectors from the total mass center to the pressure centers are assumed to be fixed, and given by [-0.17, -0.10, 4.50]$^{\mathrm{T}}$ m and [-0.17, -0.10, -9.00]$^{\mathrm{T}}$ m, respectively. Table 1 gives the initial and final boundary conditions. Several typical ZPM OCPs will be designed, and these are detailed in Table 2. Note that $h_{\max}$ is the optimization parameter in the ZPM momentum-optimal problem, and its value is intentionally changed in some numerical computations.

Table 1 The initial and final boundary conditions for the ZPM mission

Initial state	Value	Final state	Value
$\boldsymbol{\sigma}_0$	$[0.1352, -0.4144, 0.5742]^{\mathrm{T}}\times10^{-1}$	$\boldsymbol{\sigma}_f$	$[-0.3636, -0.2063, -4.1360]^{\mathrm{T}}\times10^{-1}$
$\boldsymbol{\omega}_0$ (rad/s)	$[-0.2541, -1.1145, 0.0826]^{\mathrm{T}}\times10^{-3}$	$\boldsymbol{\omega}_f$ (rad/s)	$[1.1353, 0.0030, -0.1571]^{\mathrm{T}}\times10^{-3}$
$\boldsymbol{h}_0$ (N m s)	$[-672.4768, -237.2650, -5276.7736]^{\mathrm{T}}$	$\boldsymbol{h}_f$ (N m s)	$[-12.2022, -4822.5806, -183.0330]^{\mathrm{T}}$

Table 2 The designed ZPM path planning cases

Case	Path type	Final time t_f (s)	Momentum magnitude parameter $h_{\max}$ (N m s)	Initial t_f (s)
1	Momentum-optimal	6000	Minimize $h_{\max}$	Not applicable
2	Time-optimal	Minimize t_f	1.9524×10^4	1
3	Energy-optimal	6000	1.9524×10^4	Not applicable
4	Momentum-optimal	9000	Minimize $h_{\max}$	Not applicable
5	Time-optimal	Minimize t_f	5.3427×10^3	1
6	Time-optimal	Minimize t_f	Infinity	1
7	Energy-optimal	6000	Infinity	Not applicable
8	Energy-optimal	Free	1.9524×10^4	1
9	Energy-optimal	Free	1.9524×10^4	15000

4.1 Optimal Solutions for a Single Objective

The solutions for momentum-optimal, time-optimal and energy-optimal control problems (corresponding to ZPM cases 1 to 3 in Table 2, respectively) were computed. The related results show the characteristics of different types of ZPM paths. The state solutions of the three OCPs are presented in Fig. 1. It is shown that, for the momentum-optimal and time-optimal solutions, the angular velocity changes sharply near the initial and final time. The profiles of the components of the CMGs momentum for the three solutions, $(h_{\mathrm{cmg}})_x$ and $(h_{\mathrm{cmg}})_y$, are similar, while the components $(h_{\mathrm{cmg}})_z$ are obviously different.

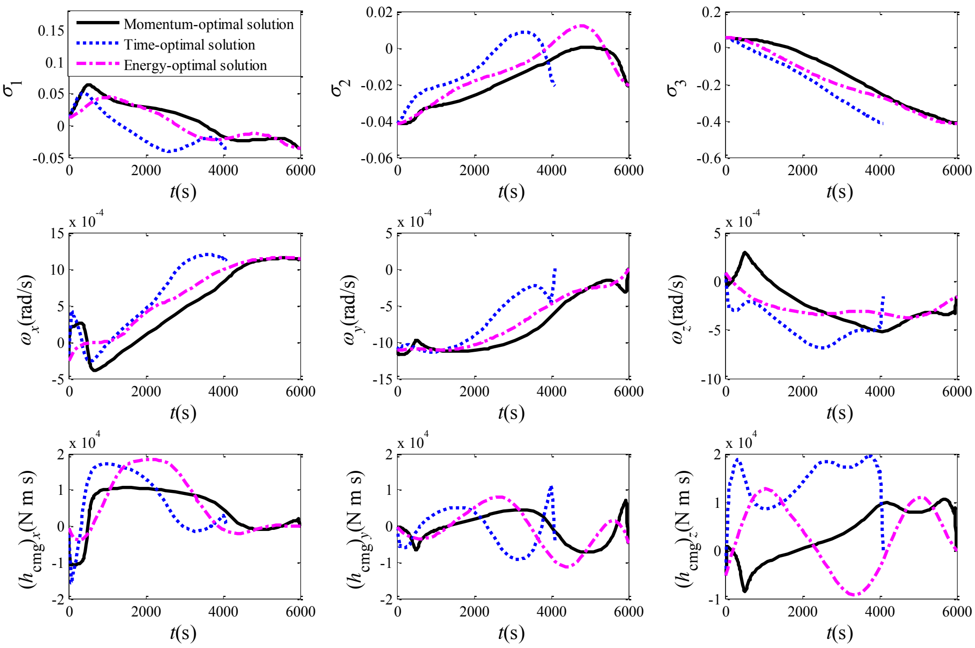

Fig. 1 The state solutions of the three ZPM OCPs

Figure 2 presents the momentum magnitude profiles and Fig. 3 presents the rate of momentum change magnitude profiles. For the energy-optimal solution, the momentum constraint is active for about 900 s, and the rate of momentum change profile is smooth. The momentum-optimal and time-optimal solutions have the same structure. The rate of momentum change constraint is active near the initial and final time, and the momentum constraint is active at intermediate times. This phenomenon may be explained physically. For the time-optimal solution, the rate of momentum change constraint is active to provide the largest control. The CMGs then maintain the maximum momentum to yield the largest possible angular velocity. At the end of the maneuver, the angular momentum of the CMGs must decrease quickly to reach the prescribed final boundary condition. So, the rate of momentum change constraint is active again. For the momentum-optimal solution, the final time is fixed and the peak momentum is maintained for as long as possible. Hence, to reduce the time for the momentum of the CMGs to change between the boundary value and the peak value, the rate of momentum change reaches the threshold, in a similar way to the time-optimal solution.

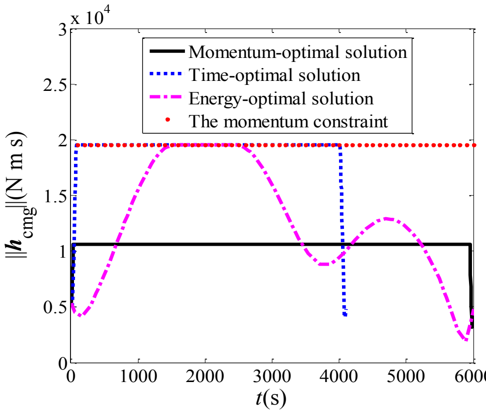

Fig. 2 The CMGs angular momentum magnitude profiles of the three ZPM OCPs

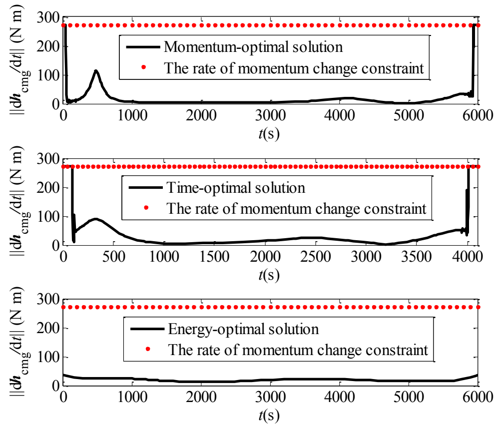

Fig. 3 The rate of CMGs angular momentum change magnitude profiles of the three ZPM OCPs

The property that the time-optimal and momentum-optimal solutions have the same structure may be accounted for mathematically, by observing that the Hamiltonians of the momentum-optimal and time-optimal control problems only differ by a constant, and the resulting optimality conditions are the same, except for the boundary conditions. In Fig. 3, it is shown that the rate of momentum change constraint is active near the initial and the final time, and this can be explained by the stationarity condition. Take the momentum-optimal control problem for example. The augmented Hamiltonian $\bar{H}$ is

$$\bar{H} := \boldsymbol{\lambda}_{\sigma}{}^{\mathrm{T}} \frac{\mathrm{d}\boldsymbol{\sigma}}{\mathrm{d}t} + \boldsymbol{\lambda}_{\omega}{}^{\mathrm{T}} \frac{\mathrm{d}\boldsymbol{\omega}}{\mathrm{d}t} + \boldsymbol{\lambda}_{h}{}^{\mathrm{T}} \frac{\mathrm{d}\boldsymbol{h}_{\mathrm{cmg}}}{\mathrm{d}t} + \lambda_{\mathrm{p1}}\left(\boldsymbol{w}^{\mathrm{T}}\boldsymbol{w} - \dot{h}_{\max}^{2}\right) + \lambda_{\mathrm{p2}}\left(\boldsymbol{h}_{\mathrm{cmg}}^{\mathrm{T}}\boldsymbol{h}_{\mathrm{cmg}} - \gamma\right), \tag{20}$$

where $\boldsymbol{\lambda}_{\sigma}$, $\boldsymbol{\lambda}_{\omega}$, and $\boldsymbol{\lambda}_{h}$ are the costate variables, and λ_{p1} and λ_{p2} are the KKT multiplier variables. Since $(\boldsymbol{J}^{-1})^{\mathrm{T}} = \boldsymbol{J}^{-1}$, the resulting stationarity condition is

$$\frac{\partial \bar{H}}{\partial \boldsymbol{w}} = \boldsymbol{\lambda}_h - \boldsymbol{J}^{-1}\boldsymbol{\lambda}_\omega + 2\lambda_{\mathrm{p1}}\boldsymbol{w} = \boldsymbol{0} \cdot \tag{21}$$

If $(\boldsymbol{\lambda}_h - \boldsymbol{J}^{-1}\boldsymbol{\lambda}_\omega) \neq \boldsymbol{0}$, then $\lambda_{\mathrm{p1}} \neq 0$, and $\|\boldsymbol{w}\|^2 = \dot{h}_{\max}^2$. If $(\boldsymbol{\lambda}_h - \boldsymbol{J}^{-1}\boldsymbol{\lambda}_\omega) = \boldsymbol{0}$, then singularity occurs and the control cannot be determined from (21). Figure 3 shows that the ZPM momentum-optimal and time-optimal control problems are singular OCPs with a singular arc in the middle.

Table 3 shows the results of the three types of ZPM solutions computed. The time-optimal solution gives the minimum time to implement the maneuver under the current CMGs capacity, and it consumes the most energy. The momentum-optimal solution gives the largest angular momentum margin for the CMGs. The rate of momentum change of the CMGs reaches the threshold for the time-optimal and momentum-optimal maneuvers. The energy-optimal solution consumes the least energy; the reduction is significant and the control profile is the smoothest.

Table 3 Results of the three optimal solutions

Case	Path type	Maneuver time (s)	Peak momentum of the CMGs (N m s)	Maneuver Energy (N^2m^2s)
1	Momentum-optimal	6000	1.0618×10^4	1.2192×10^7
2	Time-optimal	4099.9	1.9524×10^4	1.7854×10^7
3	Energy-optimal	6000	1.9524×10^4	1.2647×10^6

4.2 Peak Momentum and Maneuver Time

Bhatt [4] pointed out that a shorter maneuver time generally requires a greater momentum with respect to the momentum-optimal path. This conjecture is now proved.

Proposition 4.1 For the ZPM momentum-optimal control problem, the peak momentum monotonically decreases when the maneuver time t_f increases under the ideal TEA final boundary condition.

Proof: The Hamiltonian H of the ZPM momentum-optimal control problem is

$$H := \boldsymbol{\lambda}_\sigma^{\mathrm{T}} \frac{\mathrm{d}\boldsymbol{\sigma}}{\mathrm{d}t} + \boldsymbol{\lambda}_\omega^{\mathrm{T}} \frac{\mathrm{d}\boldsymbol{\omega}}{\mathrm{d}t} + \boldsymbol{\lambda}_h^{\mathrm{T}} \frac{\mathrm{d}\boldsymbol{h}_{\mathrm{cmg}}}{\mathrm{d}t} \cdot \tag{22}$$

According to Lemma 3.2, the sensitivity of the optimal performance $r := \min \gamma$ to the final time t_f is

$$\frac{\mathrm{d}r}{\mathrm{d}t_f} = H\big|_{t_f} = \left((\boldsymbol{\lambda}_h - \boldsymbol{J}^{-1}\boldsymbol{\lambda}_\omega)^{\mathrm{T}} \boldsymbol{w} + \boldsymbol{\lambda}_\sigma^{\mathrm{T}} \frac{\mathrm{d}\boldsymbol{\sigma}}{\mathrm{d}t} + \boldsymbol{\lambda}_\omega^{\mathrm{T}} \boldsymbol{J}^{-1}(\boldsymbol{\tau}_e - \boldsymbol{\omega}\times(\boldsymbol{J}\boldsymbol{\omega} + \boldsymbol{h}_{\mathrm{cmg}})) \right)\Bigg|_{t_f} \cdot \tag{23}$$

If the ideal TEA boundary condition is achieved at t_f, then $\left.\frac{\mathrm{d}\boldsymbol{\sigma}}{\mathrm{d}t}\right|_{t_f}=\boldsymbol{0}$ and $\left.\left(\boldsymbol{\tau}_{\mathrm{e}}-\boldsymbol{\omega}\times(\boldsymbol{J}\boldsymbol{\omega}+\boldsymbol{h}_{\mathrm{cmg}})\right)\right|_{t_f}=\boldsymbol{0}$. Substitute the stationarity condition given by (21) into (23), and note that the KKT multiplier is non-negative. Then

$$\frac{\mathrm{d}r}{\mathrm{d}t_f}=-2\lambda_{\mathrm{p1}}(t_f)\|\boldsymbol{w}\|^2\leq 0\cdot \tag{24}$$

Since r is the square of the minimum peak momentum, this proves that the peak momentum decreases as t_f increases. □

Figure 3 shows that the rate of momentum change constraint is generally active at the end of the maneuver. The KKT multiplier satisfies $\lambda_{\mathrm{p1}}(t_f)>0$, and thus $\frac{\mathrm{d}r}{\mathrm{d}t_f}=-2\lambda_{\mathrm{p1}}(t_f)\dot{h}_{\max}^2<0$. Denote the larger one of the boundary conditions of the CMGs momentum, $\|\boldsymbol{h}_0\|$ and $\|\boldsymbol{h}_f\|$, by h_{B}. Then, the case $\frac{\mathrm{d}r}{\mathrm{d}t_f}=0$ occurs when the peak momentum equals h_{B}. In this case, $\lambda_{\mathrm{p1}}(t_f)=0$, and the rate of momentum change constraint is inactive.

For the ZPM time-optimal control problem, the following conclusion may be obtained using the sensitivity analysis method.

Proposition 4.2 For the ZPM time-optimal control problem, the maneuver time $\tau:=\min t_f$ monotonically decreases when $h_{\max}$ increases, i.e. $\frac{\mathrm{d}\tau}{\mathrm{d}h_{\max}}\leq 0$. When the momentum constraint is active in the maneuver, $\frac{\mathrm{d}\tau}{\mathrm{d}h_{\max}}<0$; when the momentum constraint is inactive, $\frac{\mathrm{d}\tau}{\mathrm{d}h_{\max}}=0$.

Proof: The augmented Hamiltonian $\bar{H}$ of the ZPM time-optimal control problem is

$$\bar{H}:=1+\boldsymbol{\lambda}_{\boldsymbol{\sigma}}^{\mathrm{T}}\frac{\mathrm{d}\boldsymbol{\sigma}}{\mathrm{d}t}+\boldsymbol{\lambda}_{\boldsymbol{\omega}}^{\mathrm{T}}\frac{\mathrm{d}\boldsymbol{\omega}}{\mathrm{d}t}+\boldsymbol{\lambda}_{\boldsymbol{h}}^{\mathrm{T}}\frac{\mathrm{d}\boldsymbol{h}_{\mathrm{cmg}}}{\mathrm{d}t}+\lambda_{\mathrm{p1}}\left(\boldsymbol{w}^{\mathrm{T}}\boldsymbol{w}-\dot{h}_{\max}^2\right)+\lambda_{\mathrm{p2}}\left(\boldsymbol{h}_{\mathrm{cmg}}^{\mathrm{T}}\boldsymbol{h}_{\mathrm{cmg}}-h_{\max}^2\right)\cdot \tag{25}$$

From Lemma 3.1, and noting that $\lambda_{\mathrm{p2}}(t)\geq 0$, the sensitivity of the optimal performance $\tau:=\min t_f$ to the parameter $h_{\max}$ is

$$\frac{\mathrm{d}\tau}{\mathrm{d}h_{\max}}=\int_{t_0}^{t_f}-2\lambda_{\mathrm{p2}}h_{\max}\mathrm{d}t\leq 0\cdot \tag{26}$$

When the momentum constraint is active during the maneuver, $\lambda_{\mathrm{p2}}(t)$ will not equal zero for the whole time span, and thus $\frac{\mathrm{d}\tau}{\mathrm{d}h_{\max}} < 0$. When the momentum constraint is inactive during the maneuver, then $\lambda_{\mathrm{p2}}(t) = 0$ and so $\frac{\mathrm{d}\tau}{\mathrm{d}h_{\max}} = 0$. □

The implementation of the ZPM depends on the utilization of the environmental torque. Hence, there is a lower limit to the maneuver time even with no constraint. Furthermore, the rate of momentum change constraint may take effect and determine the minimum maneuver time. When the value of $h_{\max}$ increases, there exists an $h_{\max}^{\mathrm{U}}$ such that $\left.\frac{\mathrm{d}\tau}{\mathrm{d}h_{\max}}\right|_{h_{\max}^{\mathrm{U}}}$ becomes zero. $h_{\max}^{\mathrm{U}}$ is called the **upper limit of the momentum parameter,** and the corresponding solution is defined as the **critical time-optimal solution**, with the maneuver time denoted by t_{U}. When $h_{\max} > h_{\max}^{\mathrm{U}}$, the momentum constraint is no longer active, and the minimum maneuver time equals t_{U}. On the other hand, there may exist an $h_{\max}^{\mathrm{L}}$ such that $\left.\frac{\mathrm{d}\tau}{\mathrm{d}h_{\max}}\right|_{h_{\max}^{\mathrm{L}}}$ tends to infinity. The continuous differentiability assumption means that the maneuver is not realizable if $h_{\max}$ decreases further from $h_{\max}^{\mathrm{L}}$. $h_{\max}^{\mathrm{L}}$ is called the **lower limit of the momentum parameter** and the corresponding minimum maneuver time is denoted by t_{L}. Since, generally, the existence of a time-optimal solution is equivalent to the existence of a solution, it is reasonable to infer that $h_{\max}^{\mathrm{L}}$ equals h_{B}.

When the momentum constraint is active in the maneuver, the parameter $h_{\max}$ just equals the peak angular momentum, $\max\left(\left\|\boldsymbol{h}_{\mathrm{cmg}}(t)\right\|\right)$. For the solutions on the optimal front, if the minimum maneuver time is t_f, given a certain $h_{\max}$, the minimum peak momentum is $h_{\max}$ when the maneuver time is set to t_f, and vice versa. So, a conclusion stronger than Proposition 4.1 is obtained as follows.

Corollary 4.1 For the ZPM momentum-optimal control problem, provided the peak momentum is higher than the lower limit of the momentum parameter, the peak momentum decreases strictly monotonically as the maneuver time t_f increases under arbitrary fixed final boundary conditions.

In deducing Proposition 4.2, there was no special requirement on the final boundary conditions, so the final boundary conditions may be arbitrary in Corollary 4.1. Regarding the strict monotonicity, because the momentum constraint is active, $\frac{\mathrm{d}r}{\mathrm{d}t_f} \le 0$ is derived from $\frac{\mathrm{d}\tau}{\mathrm{d}h_{\max}} < 0$, and $\frac{\mathrm{d}r}{\mathrm{d}t_f} = 0$ occurs only when $\frac{\mathrm{d}\tau}{\mathrm{d}h_{\max}} = -\infty$. Define the momentum-optimal solution with final time equal to t_{L} as the **critical momentum-optimal solution**. Then $\left.\frac{\mathrm{d}r}{\mathrm{d}t_f}\right|_{t_{\mathrm{L}}} = 0$. The peak momentum performance will not improve, but maintain the value of $h_{\max}^{\mathrm{L}}$, even if a longer maneuver time is permitted. For the momentum-optimal maneuver with the ideal TEA final boundary condition, the critical momentum-optimal solution is the interface where the rate of momentum change constraint at the final time changes from active to inactive.

In order to seek the critical momentum-optimal solution and the critical time-optimal solution, and to verify the relation between the minimum peak momentum and the maneuver time, the ZPM cases 1, 2, 4, 5 and 6 given in Table 2 were run. Case 5 is designed to seek the critical momentum-optimal solution, and the momentum magnitude parameter given in Table 2 is $h_{\mathrm{B}} = \|\boldsymbol{h}_0\|$. Case 6 seeks the critical time-optimal solution. Figure 4 gives the momentum magnitude profiles, and shows that the peak momentum decreases as the maneuver time increases. For the critical momentum-optimal solution (case 5), the magnitude of momentum of the CMGs stays at h_{B} except for the time around t_f, and the maneuver time is t_{L}=11013.9s. For the critical time-optimal solution (case 6), the momentum profile is approximately triangular and $h_{\max}^{\mathrm{U}}$=1.32976×10^5 N m s. The corresponding maneuver time is t_{U}=1274.6s, which is restricted by the rate of momentum change constraint as shown in Fig. 5. In Fig. 5, only results for cases 4, 5 and 6 are presented because cases 1 and 2 have been given in Fig. 3. The curve for case 4 is similar to cases 1 and 2 except that the time, when the constraint is active, is shorter. For the critical momentum-optimal solution, the rate of change of the CMGs momentum reaches the threshold only around t_f. For the critical time-optimal solution, the rate of momentum change constraint is active throughout the maneuver.

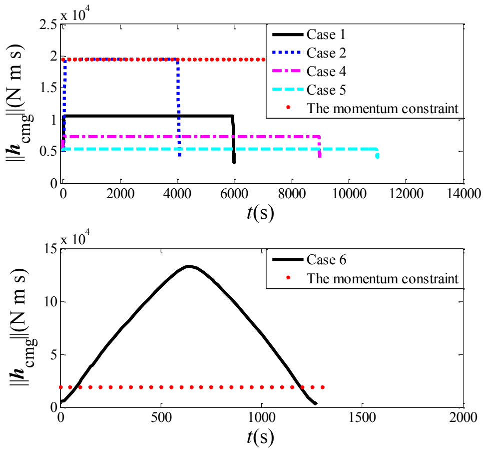

Fig. 4 The angular momentum magnitude profiles of the CMGs

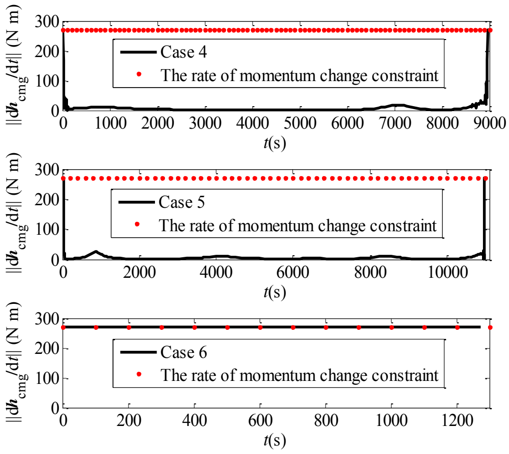

Fig. 5 The rate of angular momentum change magnitude profiles of the CMGs

The strict monotonicity in the preceding analysis means that the Pareto optimal front between the peak momentum and the maneuver time is continuous. A set of numerical computations was performed to calculate the optimal front using the constraint method [5]. The results, together with the current time-optimal solution from case 2, the critical momentum-optimal solution from case 5 and the critical time-optimal solution from case 6, are all presented in Fig. 6. Clearly, the minimum peak momentum decreases as the maneuver time increases. The optimal front is fixed by the critical time-optimal solution and critical momentum-optimal solution. The slope of the curve tends to infinity at the critical time-optimal solution and equals zero at the critical momentum-optimal solution, which is consistent with the previous analysis. Figure 7 presents the rate of momentum change at t_f with respect to the maneuver time, and shows that the rate of momentum change constraint is not active as the maneuver time increases beyond the maneuver time of the critical momentum-optimal solution.

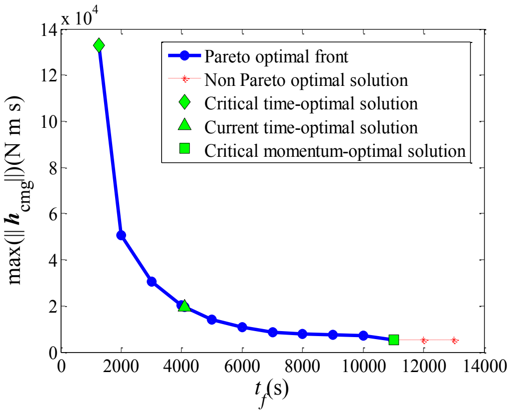

Fig. 6 The Pareto optimal front between the peak momentum and the maneuver time

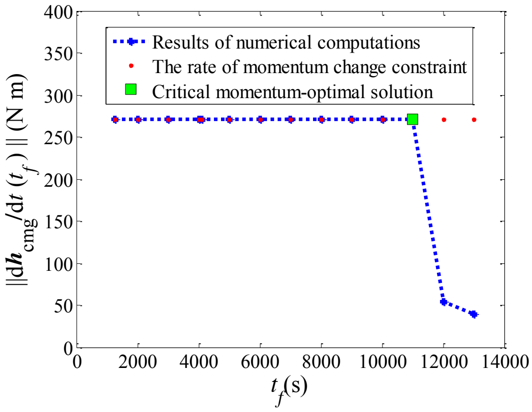

Fig. 7 The relation between the rate of momentum change of the CMGs at t_f and the maneuver time

4.3 Maneuver Energy and Peak Momentum

For the ZPM energy-optimal control problem, given the fixed maneuver time and arbitrary final boundary conditions, the conclusion below holds.

Proposition 4.3 For the ZPM energy-optimal control problem with fixed final maneuver time, the energy performance $e := \min E$ monotonically decreases when the parameter $h_{\max}$ increases, i.e. $\frac{\mathrm{d}e}{\mathrm{d}h_{\max}} \leq 0$. When the momentum constraint is active, $\frac{\mathrm{d}e}{\mathrm{d}h_{\max}} < 0$; when the momentum constraint is inactive, $\frac{\mathrm{d}e}{\mathrm{d}h_{\max}} = 0$.

According to Lemma 3.1, the deduction is similar to Proposition 4.2. When the momentum constraint is active in the maneuver, the parameter $h_{\max}$ equals the peak angular momentum, $\max\left(\left\|\boldsymbol{h}_{\mathrm{cmg}}(t)\right\|\right)$. Similarly, there is a critical angular momentum, $h_{\max}^{\mathrm{C}}$, from which $\frac{\mathrm{d}e}{\mathrm{d}h_{\max}}=0$. The corresponding solution is defined as the **critical energy-optimal solution**, and its energy performance is denoted by e_{C}, which represents the minimum energy consumed under the given boundary conditions and maneuver time when the momentum constraint is neglected. When $h_{\max} < h_{\max}^{\mathrm{C}}$, the momentum magnitude constraint is active. When $h_{\max} \geq h_{\max}^{\mathrm{C}}$, this constraint is inactive and the energy consumed will not be changed.

The ZPM cases 3 and 7 in Table 2 were run. Case 7 is designed for the critical energy-optimal solution. In Fig. 8, the momentum constraint of case 3 is active during the maneuver. The result for case 7 shows that the peak momentum of the critical energy-optimal solution under the set maneuver time and boundary conditions is $h_{\max}^{\mathrm{C}}=2.5985\times10^4$ N m s. Figure 9 shows that the rate of momentum change constraint is not violated, and the profiles are smooth. The energy performance metric for case 3 is E=1.2647×10^6 N^{2}m^{2}s, and for case 7 is E=1.1007×10^6 N^{2}m^{2}s, which is the value of e_{C}.

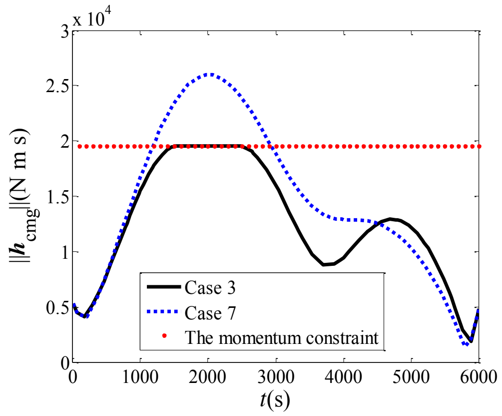

Fig. 8 The angular momentum magnitude profiles of the CMGs

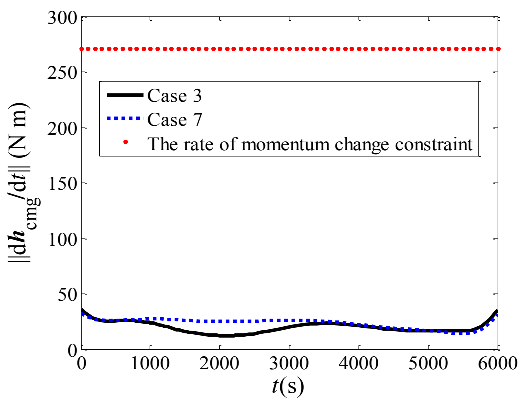

Fig. 9 The rate of angular momentum change magnitude profiles of the CMGs

The Pareto optimal front between the maneuver energy and the peak momentum was also computed by the constraint method. Note that the final time is fixed at 6000s. Figure 10 shows the optimal front, together with the momentum-optimal solution from case 1, the current energy-optimal solution from case 3 and the critical energy-optimal solution from case 7. As expected, the minimum maneuver energy decreases when the peak momentum increases for a fixed t_f. The front is bounded by the momentum-optimal solution and the critical energy-optimal solution. The slope of the curve tends to infinity at the momentum-optimal solution and the slope is zero at the critical energy-optimal solution.

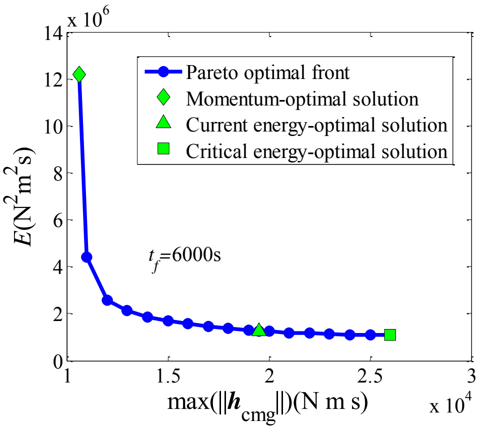

Fig. 10 The Pareto optimal front between maneuver energy and peak momentum

4.4 Maneuver Energy and Maneuver Time

For the ZPM energy-optimal control problem, it will be shown that the maneuver energy does not decrease monotonically as the maneuver time increases, even under the ideal TEA final boundary condition. According to Lemma 3.2, the sensitivity is

$$\frac{\mathrm{d}e}{\mathrm{d}t_f} = H\big|_{t_f} = \left((\boldsymbol{w}+\boldsymbol{\omega}\times\boldsymbol{h}_{\mathrm{cmg}})^{\mathrm{T}}(\boldsymbol{w}+\boldsymbol{\omega}\times\boldsymbol{h}_{\mathrm{cmg}}) + \boldsymbol{\lambda}_{\sigma}{}^{\mathrm{T}}\frac{\mathrm{d}\boldsymbol{\sigma}}{\mathrm{d}t} + \boldsymbol{\lambda}_{\omega}{}^{\mathrm{T}}\frac{\mathrm{d}\boldsymbol{\omega}}{\mathrm{d}t} + \boldsymbol{\lambda}_{h}{}^{\mathrm{T}}\frac{\mathrm{d}\boldsymbol{h}_{\mathrm{cmg}}}{\mathrm{d}t} \right)\Bigg|_{t_f} . \tag{27}$$

The augmented Hamiltonian $\bar{H}$ of the ZPM energy-optimal control problem is

$$\begin{aligned}\bar{H} := {}& (\boldsymbol{w}+\boldsymbol{\omega}\times\boldsymbol{h}_{\mathrm{cmg}})^{\mathrm{T}}(\boldsymbol{w}+\boldsymbol{\omega}\times\boldsymbol{h}_{\mathrm{cmg}}) + \boldsymbol{\lambda}_{\sigma}{}^{\mathrm{T}}\frac{\mathrm{d}\boldsymbol{\sigma}}{\mathrm{d}t} + \boldsymbol{\lambda}_{\omega}{}^{\mathrm{T}}\frac{\mathrm{d}\boldsymbol{\omega}}{\mathrm{d}t} + \boldsymbol{\lambda}_{h}{}^{\mathrm{T}}\frac{\mathrm{d}\boldsymbol{h}_{\mathrm{cmg}}}{\mathrm{d}t} ,\\ & + \lambda_{\mathrm{p1}}\left(\boldsymbol{w}^{\mathrm{T}}\boldsymbol{w} - \dot{h}_{\max}^2\right) + \lambda_{\mathrm{p2}}\left(\boldsymbol{h}_{\mathrm{cmg}}^{\mathrm{T}}\boldsymbol{h}_{\mathrm{cmg}} - h_{\max}^2\right)\end{aligned} \tag{28}$$

and the resulting stationarity condition is

$$\frac{\partial \bar{H}}{\partial \boldsymbol{w}} = 2(\boldsymbol{w}+\boldsymbol{\omega}\times\boldsymbol{h}_{\mathrm{cmg}}) - \boldsymbol{J}^{-1}\boldsymbol{\lambda}_{\omega} + \boldsymbol{\lambda}_{h} + 2\lambda_{\mathrm{p1}}\boldsymbol{w} = \boldsymbol{0} . \tag{29}$$

Two situations are now discussed, which depend on whether the rate of momentum change constraint is active or not. If the rate of momentum change constraint at t_f is active, then substituting the stationarity condition given by (29) into (27), together with the ideal TEA final boundary condition, i.e. $\left.\frac{\mathrm{d}\boldsymbol{\sigma}}{\mathrm{d}t}\right|_{t_f}=\boldsymbol{0}$ and $\left.\left(\boldsymbol{\tau}_e-\boldsymbol{\omega}\times(\boldsymbol{J}\boldsymbol{\omega}+\boldsymbol{h}_{\mathrm{cmg}})\right)\right|_{t_f}=\boldsymbol{0}$, gives

$$\frac{\mathrm{d}e}{\mathrm{d}t_f}=-\boldsymbol{u}_f^{\mathrm{T}}\boldsymbol{u}_f+2\boldsymbol{u}_f^{\mathrm{T}}(\boldsymbol{\omega}_f\times\boldsymbol{h}_f)-2\lambda_{\mathrm{p1}}(t_f)\dot{h}_{\max}^2, \tag{30}$$

where $\boldsymbol{u}_f$ is the abbreviation of $\boldsymbol{u}(t_f)$. Here, $\boldsymbol{w}$ is replaced by $\boldsymbol{w}=\boldsymbol{u}-\boldsymbol{\omega}\times\boldsymbol{h}_{\mathrm{cmg}}$ for simplicity. If the rate of momentum change constraint at t_f is not active, then $\lambda_{\mathrm{p1}}(t_f)=0$, and hence

$$\frac{\mathrm{d}e}{\mathrm{d}t_f}=-\boldsymbol{u}_f^{\mathrm{T}}\boldsymbol{u}_f+2\boldsymbol{u}_f^{\mathrm{T}}(\boldsymbol{\omega}_f\times\boldsymbol{h}_f). \tag{31}$$

In (30), since $\|\boldsymbol{w}\|=\dot{h}_{\max}$, it is straightforward to verify that $-\boldsymbol{u}_f^{\mathrm{T}}\boldsymbol{u}_f+2\boldsymbol{u}_f^{\mathrm{T}}(\boldsymbol{\omega}_f\times\boldsymbol{h}_f)<0$ using the data given in Table 1. Thus, $\frac{\mathrm{d}e}{\mathrm{d}t_f}<0$. In (31), the sign of $\frac{\mathrm{d}e}{\mathrm{d}t_f}$ cannot be determined. Thus, the energy performance can also increase as the maneuver time increases. This is because the maintenance of the final angular momentum of the CMGs still consumes energy, i.e. $\boldsymbol{u}=\boldsymbol{\omega}_f\times\boldsymbol{h}_f\neq\boldsymbol{0}$. The energy-optimal solution that satisfies $\frac{\mathrm{d}e}{\mathrm{d}t_f}=0$ is defined as the **extremum energy-optimal solution**.

In contrast, if we introduce a pseudo energy performance index given by

$$\tilde{E}:=\int_{t_0}^{t_f}\boldsymbol{w}^{\mathrm{T}}\boldsymbol{w}\,\mathrm{d}t, \tag{32}$$

with the similar analysis as above, it may be proved that the optimal value of this performance index, denoted as $\tilde{e}:=\min\tilde{E}$, decreases when the maneuver time t_f increases under the ideal TEA final boundary condition.

A set of ZPM energy-optimal problems with different fixed maneuver time was solved numerically to obtain the relation curve between the minimum energy and maneuver time. Especially, the two ZPM cases 7 and 8 in Table 2 were used to seek possible extrema energy-optimal solutions. Figure 11 shows that the curve is not monotonic and that the Pareto optimal front (the solid line) between the maneuver energy and maneuver time is discontinuous. There are two extrema energy-optimal solutions. The first appears when the maneuver time is 9049.7s, with an energy performance of $4.4340\times10^5\ \mathrm{N^2m^2s}$. The second happens at 15358.5s with an energy performance of $2.3640\times10^5\ \mathrm{N^2m^2s}$. Generally, the minimum energy decreases as the maneuver time increases. This occurs because in

(31), $\boldsymbol{\omega}_f \times \boldsymbol{h}_f$ is a small quantity, and thus $\dfrac{\mathrm{d}e}{\mathrm{d}t_f} < 0$ holds for most of time. The relation between peak momentum and maneuver time in the energy-optimal solutions is presented in Fig. 12. The curve is complex. It is shown that before a maneuver time of 7500s the momentum magnitude threshold is reached, and then the peak momentum keeps decreasing before the first extremum energy-optimal solution.

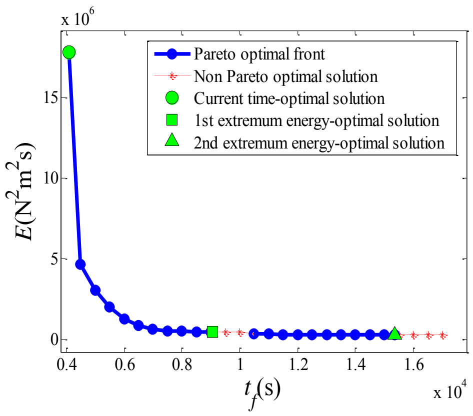

Fig. 11 The Pareto optimal front between maneuver energy and maneuver time

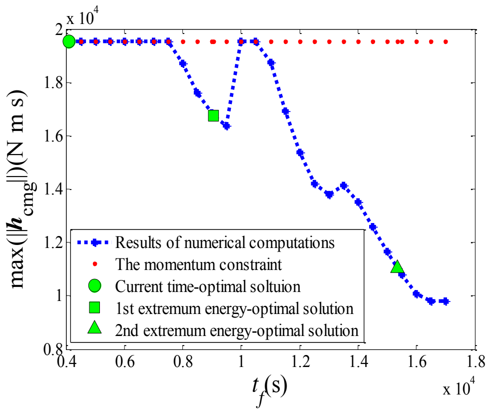

Fig. 12 The relation between peak momentum and maneuver time for the energy-optimal solutions

4.5 Synthesis of the ZPM MOP

As three objectives are involved in the ZPM MOP, the Pareto optimal front is a surface. The investigation above was performed considering pairs of objectives, and the results will be synthesized in this subsection. In practice, long maneuver times can cause problems for the space station power and thermal safety. The minimum peak momentum and the minimum energy consumed change marginally when the maneuver time is near t_{me}, which denotes the maneuver time of the first extremum energy-optimal solution. Denote the minimum maneuver time as t_{mt}. Paths with maneuver times in the span $[t_{\mathrm{mt}}, t_{\mathrm{me}}]$ may be considered as practical paths. Let $\tilde{h}_{\max}$ be the current momentum magnitude parameter of the CMGs and h_{me} be the peak momentum of the first extremum energy-optimal solution. For the ZPM mission with boundary conditions given in Table 1, two synthesized sketches, which describe the relations among minimum maneuver energy, minimum peak momentum and maneuver time, are now presented. They are also heuristic for other ZPM missions.

In Fig. 13, on each curve the maneuver time is fixed. The left end point and the right end point of each curve represent the momentum-optimal solution and the critical energy-optimal solution, respectively. The Pareto solutions located on the dashed line are not available under current CMGs capacity. In Fig. 14, on each curve the momentum magnitude parameter of the CMGs is fixed. Along the thick lines the momentum constraint is active during the maneuver, i.e. $h_{\max}=\max\left(\left\|\boldsymbol{h}_{\mathrm{cmg}}(t)\right\|\right)$; along the thin line this constraint is not active, and the peak momentum decreases gradually. The left end points represent the time-optimal solutions under different momentum magnitude parameters, while the rightmost point of intersection is the extremum energy-optimal solution.

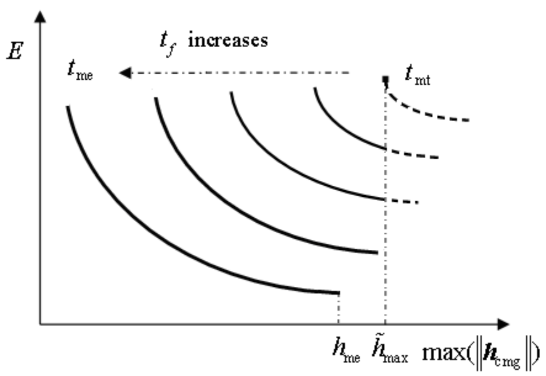

Fig. 13 The variation in the Pareto front as the maneuver time varies

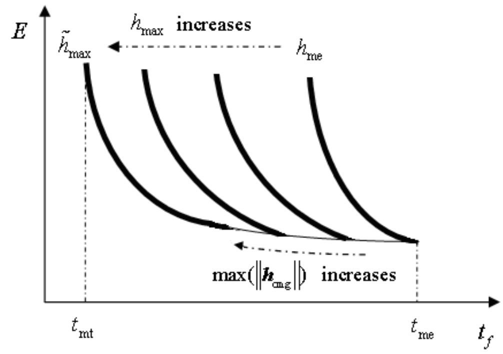

Fig. 14 The variation in the Pareto front as the maximum momentum varies

For the three types of ZPM paths, the energy-optimal path is the most favorable because of its smooth control profile and energy-saving property. However, for practical flight, sufficient angular momentum redundancy of the

CMGs is necessary. Figures 13 and 14 show the tradeoff relations among performance indices, and these may be used for the compromise design of the ZPM path.

5 Conclusion

Three types of Zero Propellant Maneuver (ZPM) paths are considered: (i) momentum-optimal, (ii) time-optimal and, (iii) energy-optimal. For the ZPM momentum-optimal control problem, the minimum peak momentum of Control Momentum Gyroscopes (CMGs) is shown to decrease as the maneuver time increases under ideal Torque Equilibrium Attitude (TEA) final boundary conditions. Indeed, the minimum peak momentum decreases as the maneuver time increases under arbitrary fixed final boundary conditions. For the ZPM time-optimal control problem, the minimum maneuver time decreases as the momentum magnitude parameter of the CMGs increases. For the ZPM energy-optimal control problem, the minimum energy consumed will decrease if a larger CMGs momentum is available. The minimum energy consumed does not monotonically decrease as the maneuver time increases, and there could be several local extrema. However, the minimum energy generally decreases while the corresponding peak momentum may change in a complex way. The Pareto optimal fronts between the peak momentum and the maneuver time, and between the maneuver energy and the peak momentum are continuous, while the front between the energy and the maneuver time is discontinuous.

Among the three path types, the typical ZPM momentum-optimal solution and time-optimal solution possess the same structure, and they are singular. The energy-optimal path could save significant energy and the control profile is smooth, and thus is a reasonable choice for the ZPM. For a specific ZPM case, the Multi-objective Optimization Problem (MOP) is synthesized and conditioned simplified sketches of the Pareto optimal fronts are presented. The sensitivity analysis method may be used to study the influence of parameter changes on the objective, and applied to study the Pareto optimal front. By taking advantage of the properties of boundary conditions and KKT multipliers, the first order sensitivity may be used to give insight into the solutions to the ZPM MOP.

The present paper uses heuristic methods, looking forward to a rigorous method. To this end, a promising approach is the one proposed in [12], which is based on image space analysis and separation theorems. It is able to find all the Pareto solutions and, overall, to optimize a scalar function over the Pareto set, without requiring to find it explicitly. Due to its theoretical relevance, the latter approach is extremely interesting and will be studied in a forthcoming paper.

References

1. Bedrossian, N., Bhatt, S., Lammers, M., Nguyen, L., Zhang, Y.: First ever flight demonstration of zero propellant maneuver attitude control concept. In: 2007 AIAA GN&C Conference, Hilton Head, SC, USA, AIAA 2007-6734 (2007)
2. Bedrossian, N., Bhatt, S., Lammers, M., Nguyen, L.: Zero propellant maneuver flight results for 180° ISS rotation. In: 2007 International Symposium on Space Flight Dynamics, Annapolis, MD, USA, NASA/CP-2007-214158 (2007)
3. Bedrossian, N., Bhatt, S., Kang W., Ross, I.M.: Zero-propellant maneuver guidance. IEEE Contr. Syst. Mag. 29(5), 53-73 (2009)
4. Bhatt, S.: Optimal reorientation of spacecraft using only control moment gyroscopes. Master's thesis, Rice University, USA (2007)
5. Zitzler, E.: Evolutionary algorithms for multiobjective optimization: methods and applications. Ph.D. dissertation, Swiss Federal Institute of Technology Zurich, Swiss (1999)
6. Rao, A.V., Benson, D.A., Darby C.L., Patterson, M.A., Francolin, C., Sanders, I., Huntington, G.T.: GPOPS: a MATLAB software for solving multiple-phase optimal control problems using the gauss pseudospectral method. ACM T. Math. Software 37(2), 1-39 (2010)
7. Garg, D., Patterson, M.A., Hager, W.W., Rao, A.V., Benson, D.A., Huntington, G.T.: A unified framework for the numerical solution of optimal control problems using pseudospectral methods. Automatica 46(11), 1843-1851 (2010)
8. Schaub, H., Junkins, J.L.: Stereographic orientation parameters or attitude dynamics a generalization of the rodrigues parameters. J. Astronaut. Sci. 44(1), 1-19 (1996)
9. Rehbock, V., Teo, K.L., Jennings, L.S.: A computational procedure for suboptimal robust controls. Dynam. Control 2, 331-348 (1992)
10. Pesch, H.J.: The accessory minimum problem and its importance for the numerical computation of closed-loop controls. In: Proceedings of the 29th IEEE Conference on Decision and Control, Honolulu, Hawaii, USA. pp. 952–953 (1990)
11. Hartl, R.F., Sethi, S.P., Vickson, R.G.: A survey of the maximum principles for optimal control problems with state constraint. SIAM Rev. 37(2), 181-218 (1995)

12. Giannessi, F., Mastroeni, G., Pellegrini, L.: On the theory of vector optimization and variational inequalities. image space analysis and separation. In: Giannessi, F. (eds.): Vector Variational Inequalities and Vector Equilibria.Mathematical Theories, Series Nonconvex Optimization and its Applications, Vol.38, pp.141-215. Kluwer, Dordrecht (2000)

Tables

Table 1 The initial and final boundary conditions for the ZPM mission

Initial state	Value	Final state	Value
$\boldsymbol{\sigma}_0$	$[0.1352, -0.4144, 0.5742]^{T} \times 10^{-1}$	$\boldsymbol{\sigma}_f$	$[-0.3636, -0.2063, -4.1360]^{T} \times 10^{-1}$
$\boldsymbol{\omega}_0$ (rad/s)	$[-0.2541, -1.1145, 0.0826]^{T} \times 10^{-3}$	$\boldsymbol{\omega}_f$ (rad/s)	$[1.1353, 0.0030, -0.1571]^{T} \times 10^{-3}$
$\boldsymbol{h}_0$ (N m s)	$[-672.4768, -237.2650, -5276.7736]^{T}$	$\boldsymbol{h}_f$ (N m s)	$[-12.2022, -4822.5806, -183.0330]^{T}$

Table 2 The designed ZPM path planning cases

Case	Path type	Final time t_f (s)	Momentum magnitude parameter $h_{\max}$ (N m s)	Initial t_f (s)
1	Momentum-optimal	6000	Minimize $h_{\max}$	Not applicable
2	Time-optimal	Minimize t_f	1.9524×10^{4}	1
3	Energy-optimal	6000	1.9524×10^{4}	Not applicable
4	Momentum-optimal	9000	Minimize $h_{\max}$	Not applicable
5	Time-optimal	Minimize t_f	5.3427×10^{3}	1
6	Time-optimal	Minimize t_f	Infinity	1
7	Energy-optimal	6000	Infinity	Not applicable
8	Energy-optimal	Free	1.9524×10^{4}	1
9	Energy-optimal	Free	1.9524×10^{4}	15000

Table 3 Results of the three optimal solutions

Case	Path type	Maneuver time (s)	Peak momentum of the CMGs(N m s)	Maneuver Energy (N^2m^2s)
1	Momentum-optimal	6000	1.0618×10^{4}	1.2192×10^{7}
2	Time-optimal	4099.9	1.9524×10^{4}	1.7854×10^{7}
3	Energy-optimal	6000	1.9524×10^{4}	1.2647×10^{6}

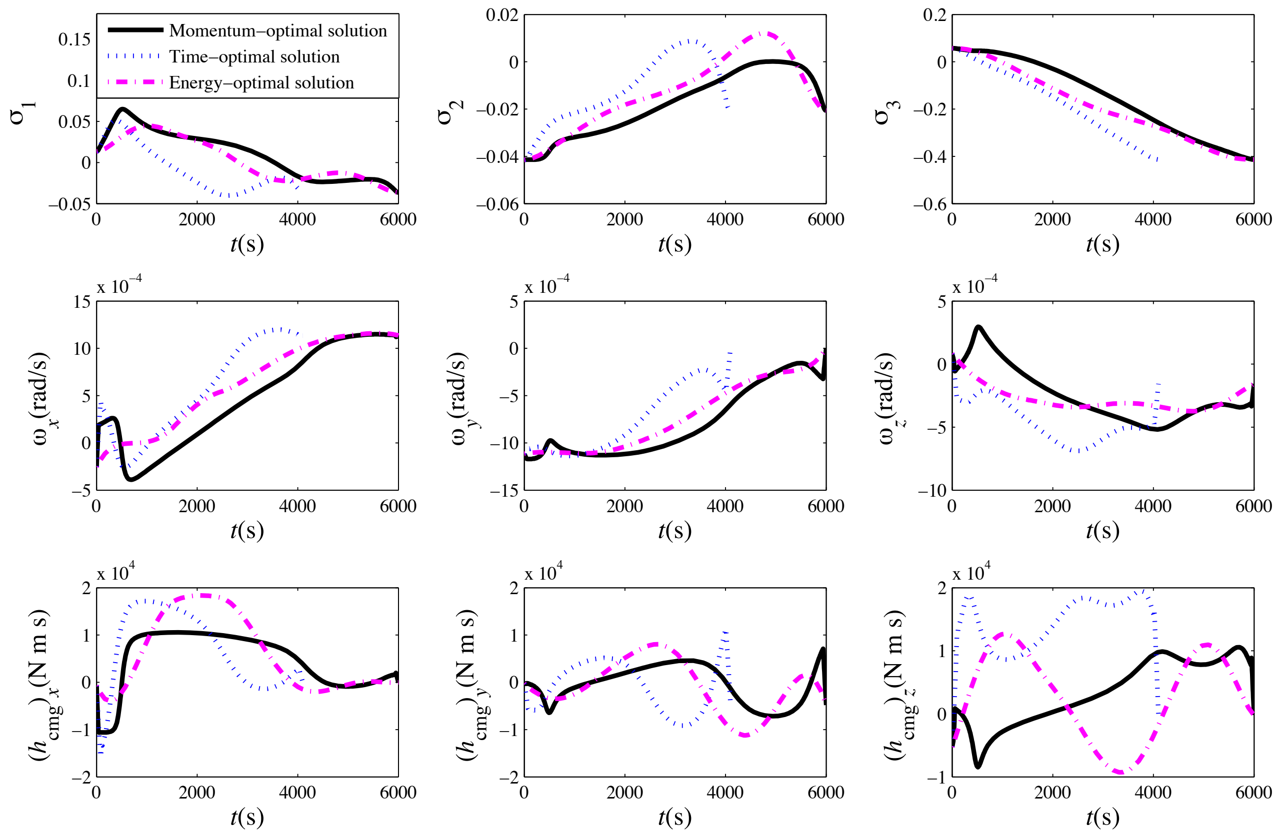
Momentum–optimal solution
Time–optimal solution
Energy–optimal solution
σ1
σ2
σ3
ωx(rad/s)
ωy(rad/s)
ωz(rad/s)
(hcmg)x(N m s)
(hcmg)y(N m s)
(hcmg)z(N m s)
t(s)
x 10−4
x 10^4

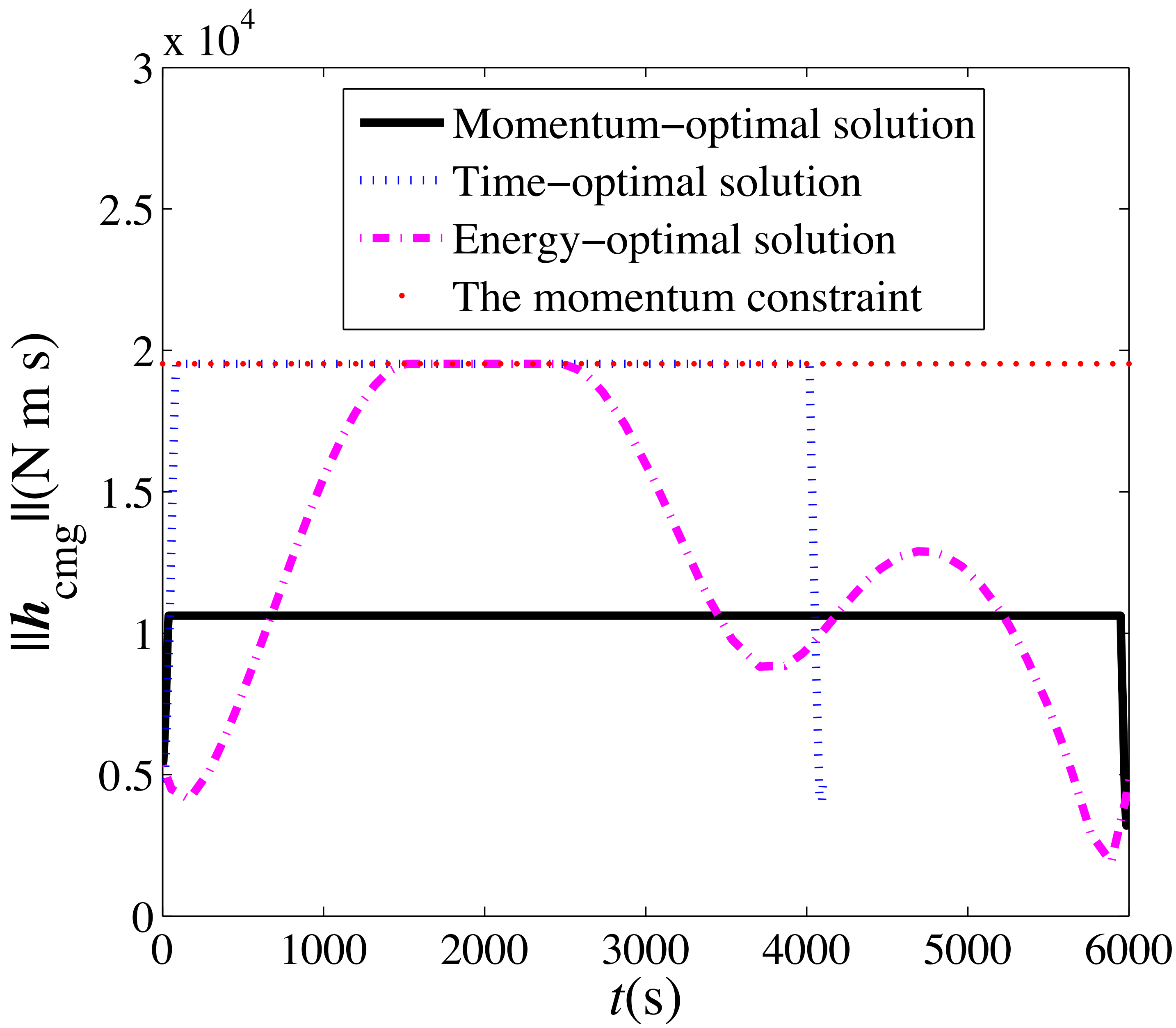

x 10^4
3
2.5
2
1.5
1
0.5
0
0
1000
2000
3000
4000
5000
6000
t(s)
||h_cmg||(N m s)
Momentum−optimal solution
Time−optimal solution
Energy−optimal solution
The momentum constraint

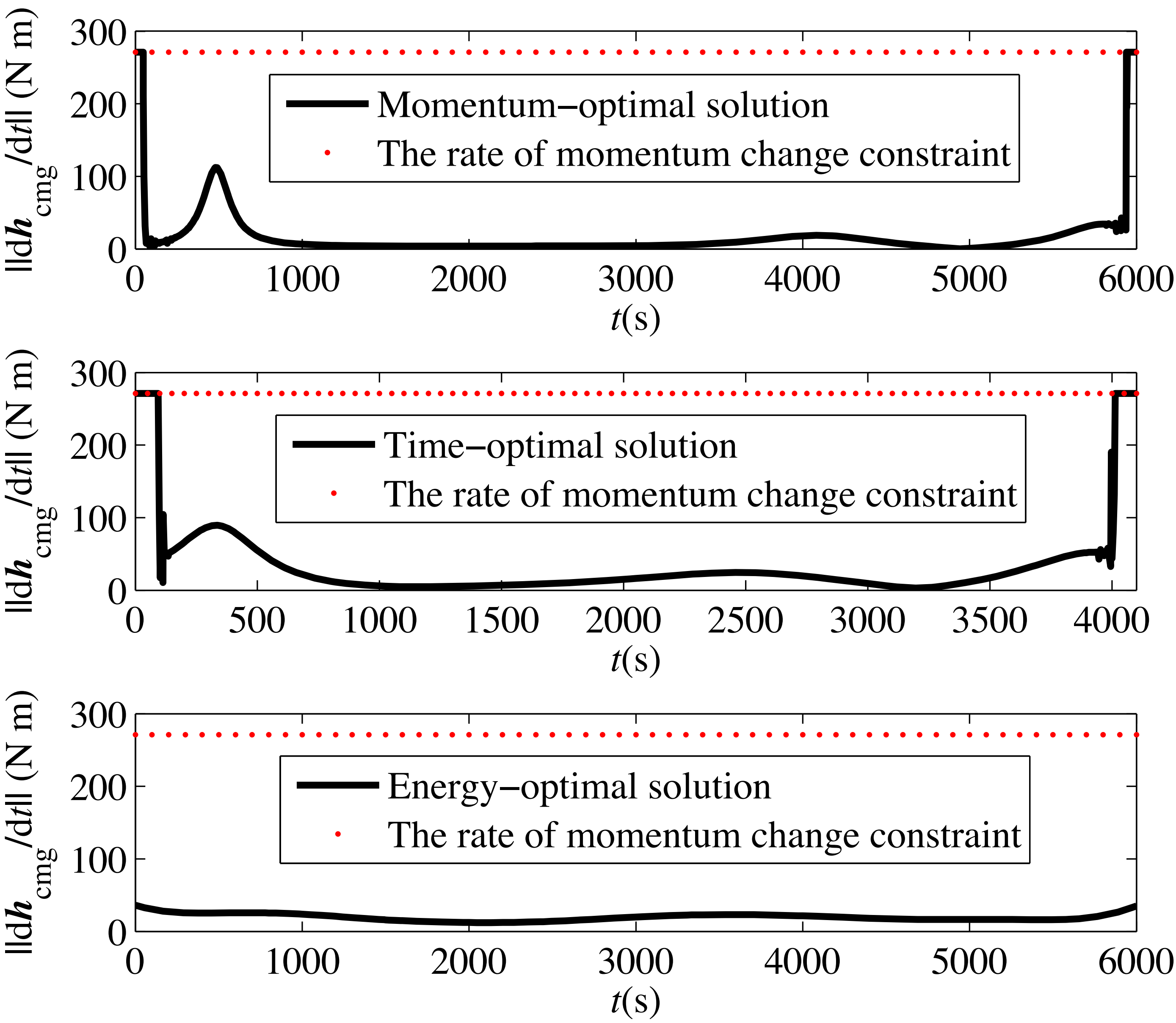

Momentum−optimal solution
The rate of momentum change constraint
Time−optimal solution
The rate of momentum change constraint
Energy−optimal solution
The rate of momentum change constraint
$\|\mathrm{d}\boldsymbol{h}_{\mathrm{cmg}}/\mathrm{d}t\|$ (N m)
t(s)

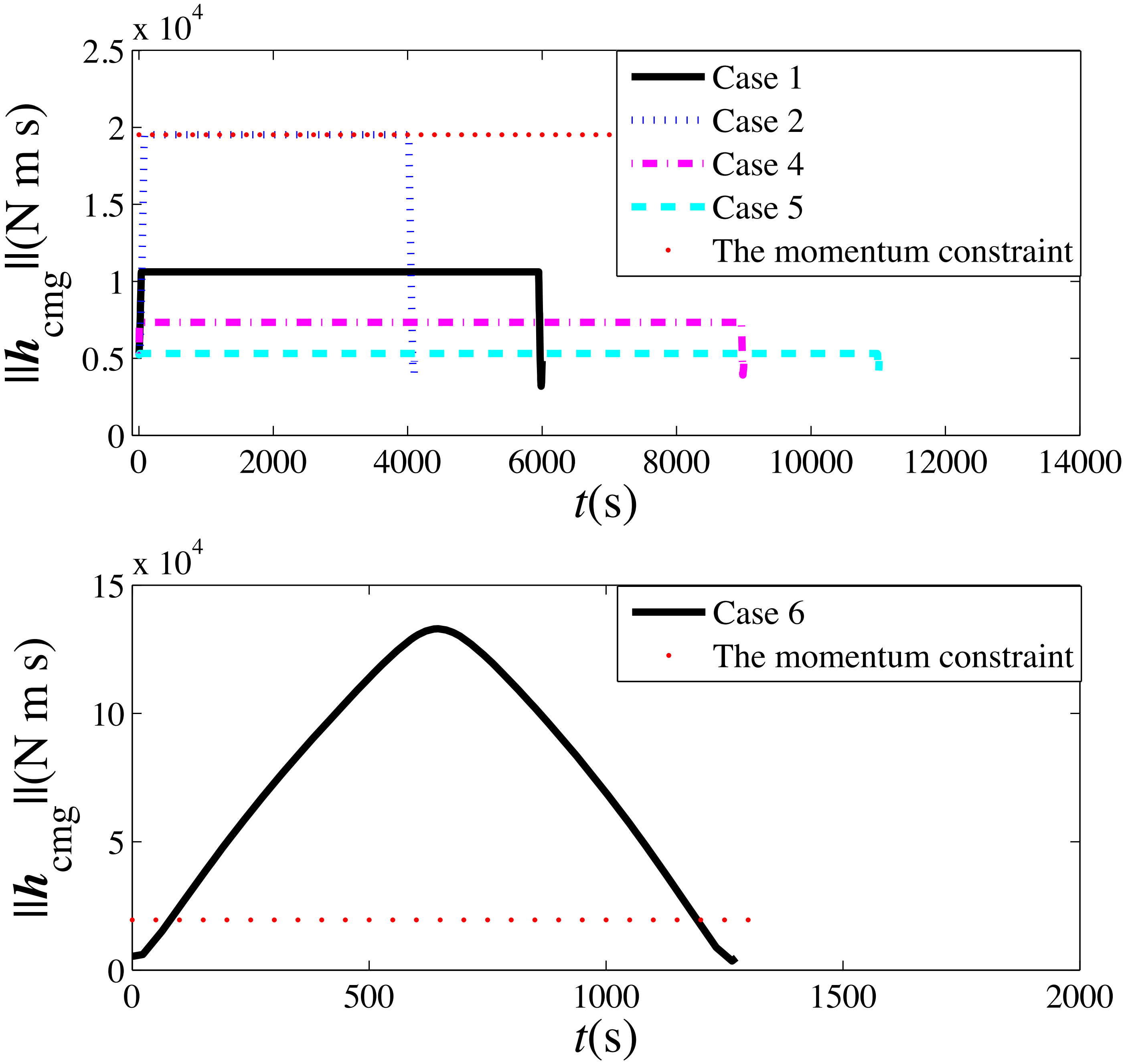
x 10^4
2.5
2
1.5
1
0.5
0
||h_cmg||(N m s)
0
2000
4000
6000
8000
10000
12000
14000
t(s)
Case 1
Case 2
Case 4
Case 5
The momentum constraint
x 10^4
15
10
5
0
||h_cmg||(N m s)
0
500
1000
1500
2000
t(s)
Case 6
The momentum constraint

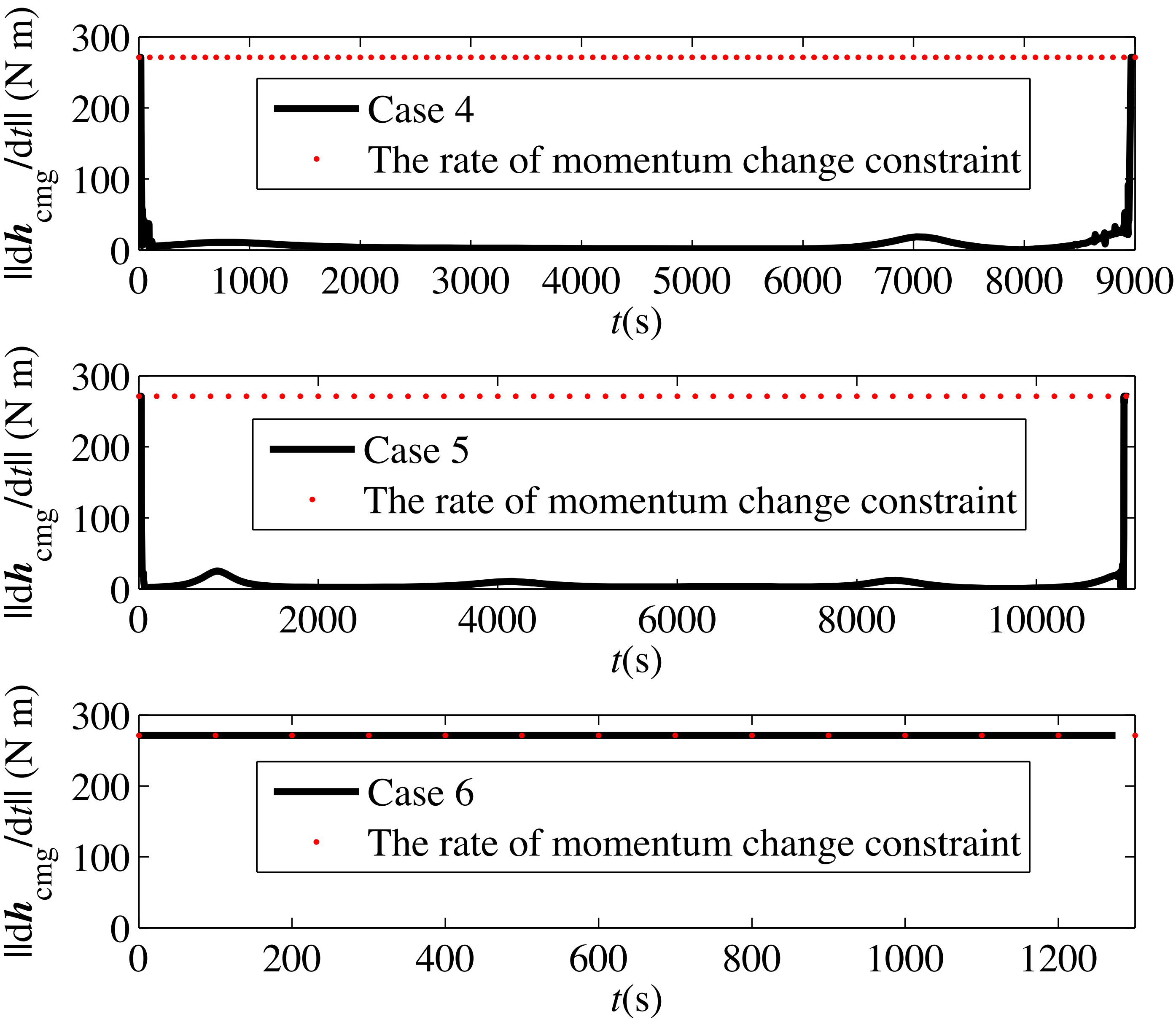

Case 4
The rate of momentum change constraint
Case 5
The rate of momentum change constraint
Case 6
The rate of momentum change constraint
$\|\mathrm{d}\boldsymbol{h}_{\mathrm{cmg}}/\mathrm{d}t\|$ (N m)
t(s)

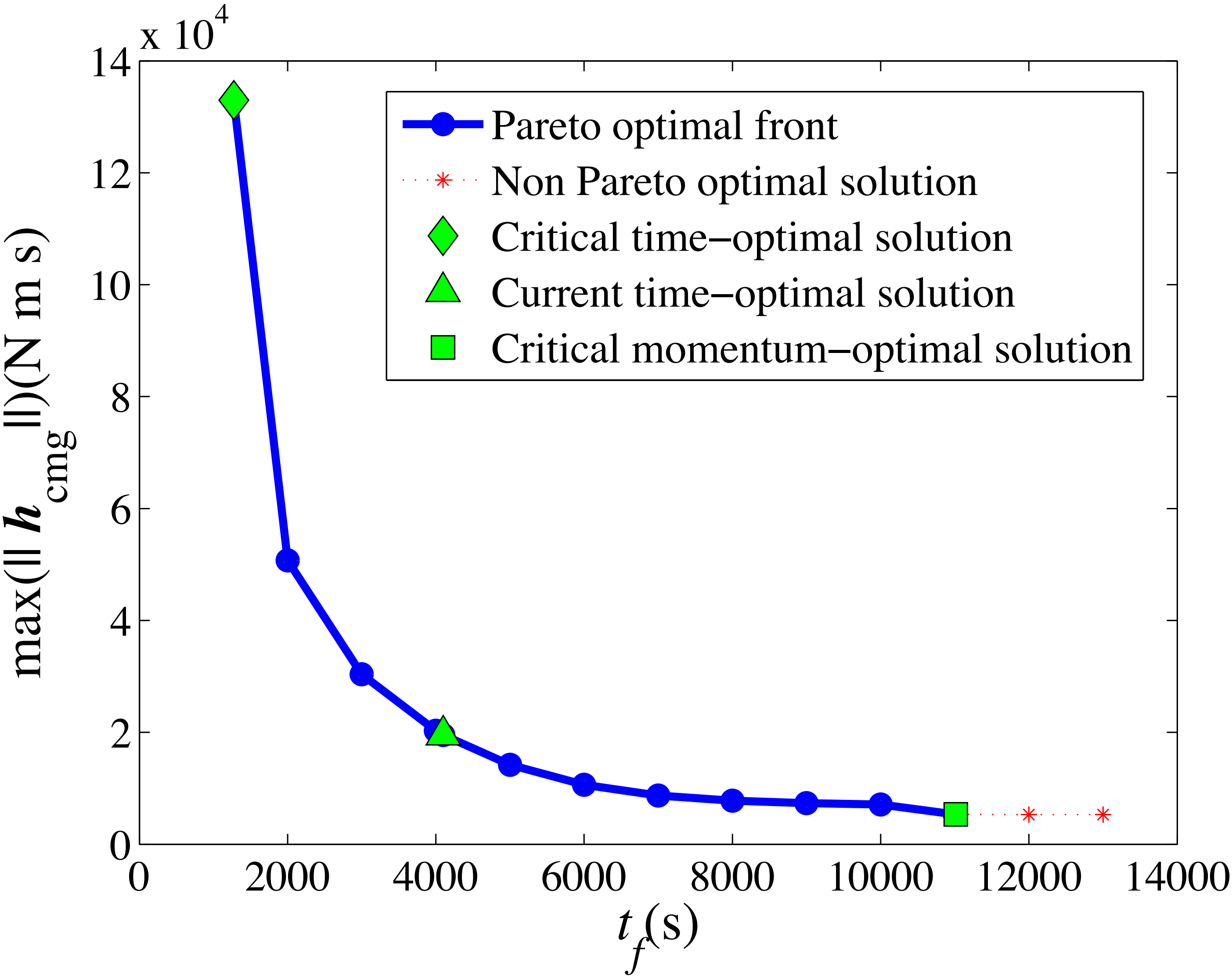

x 10^4
14
12
10
8
6
4
2
0
max(|| h cmg ||)(N m s)
0
2000
4000
6000
8000
10000
12000
14000
t f (s)
Pareto optimal front
Non Pareto optimal solution
Critical time−optimal solution
Current time−optimal solution
Critical momentum−optimal solution

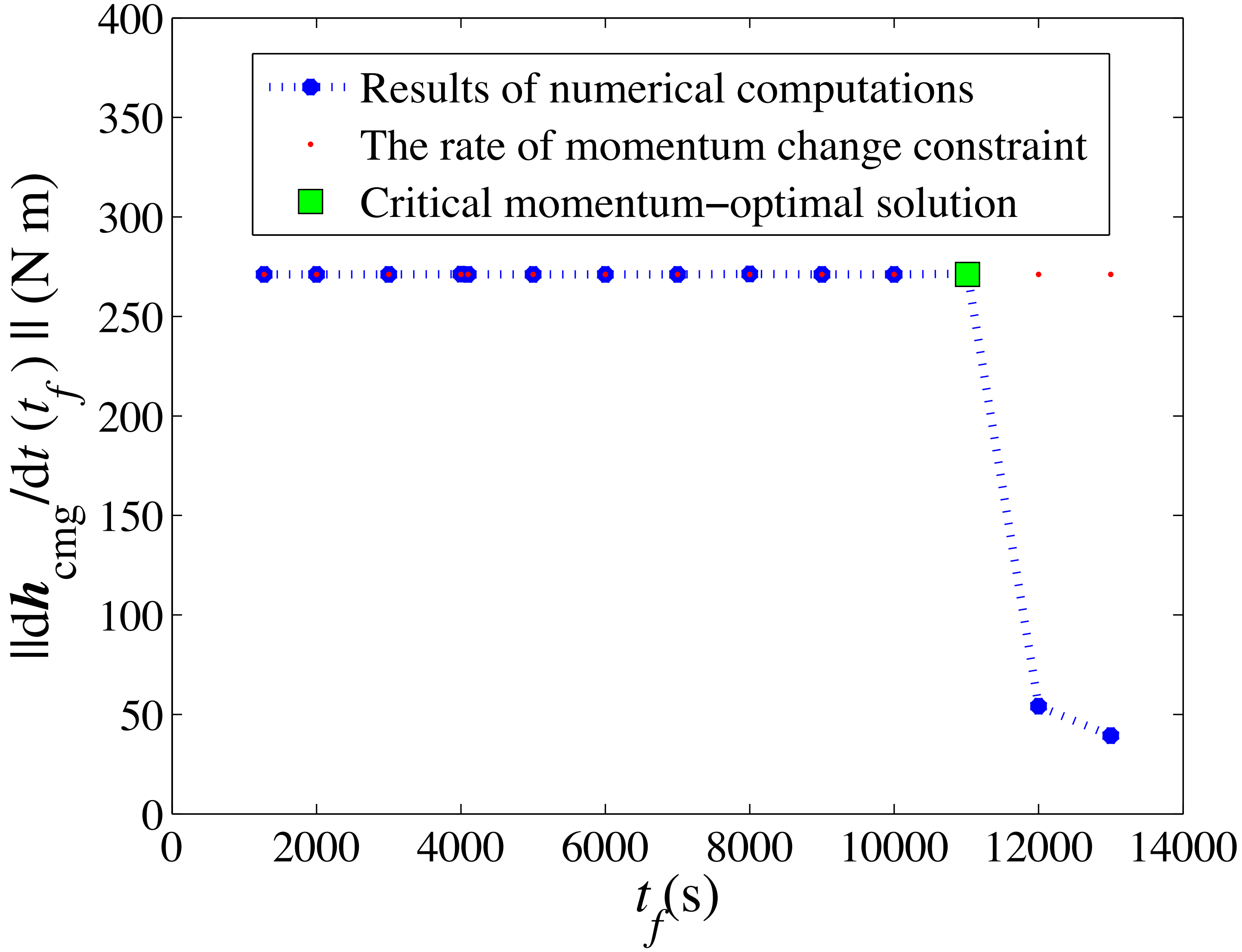
Results of numerical computations
The rate of momentum change constraint
Critical momentum−optimal solution
$\|\mathrm{d}\boldsymbol{h}_{\mathrm{cmg}}/\mathrm{d}t\,(t_f)\|$ (N m)
t_f(s)
0
50
100
150
200
250
300
350
400
0
2000
4000
6000
8000
10000
12000
14000

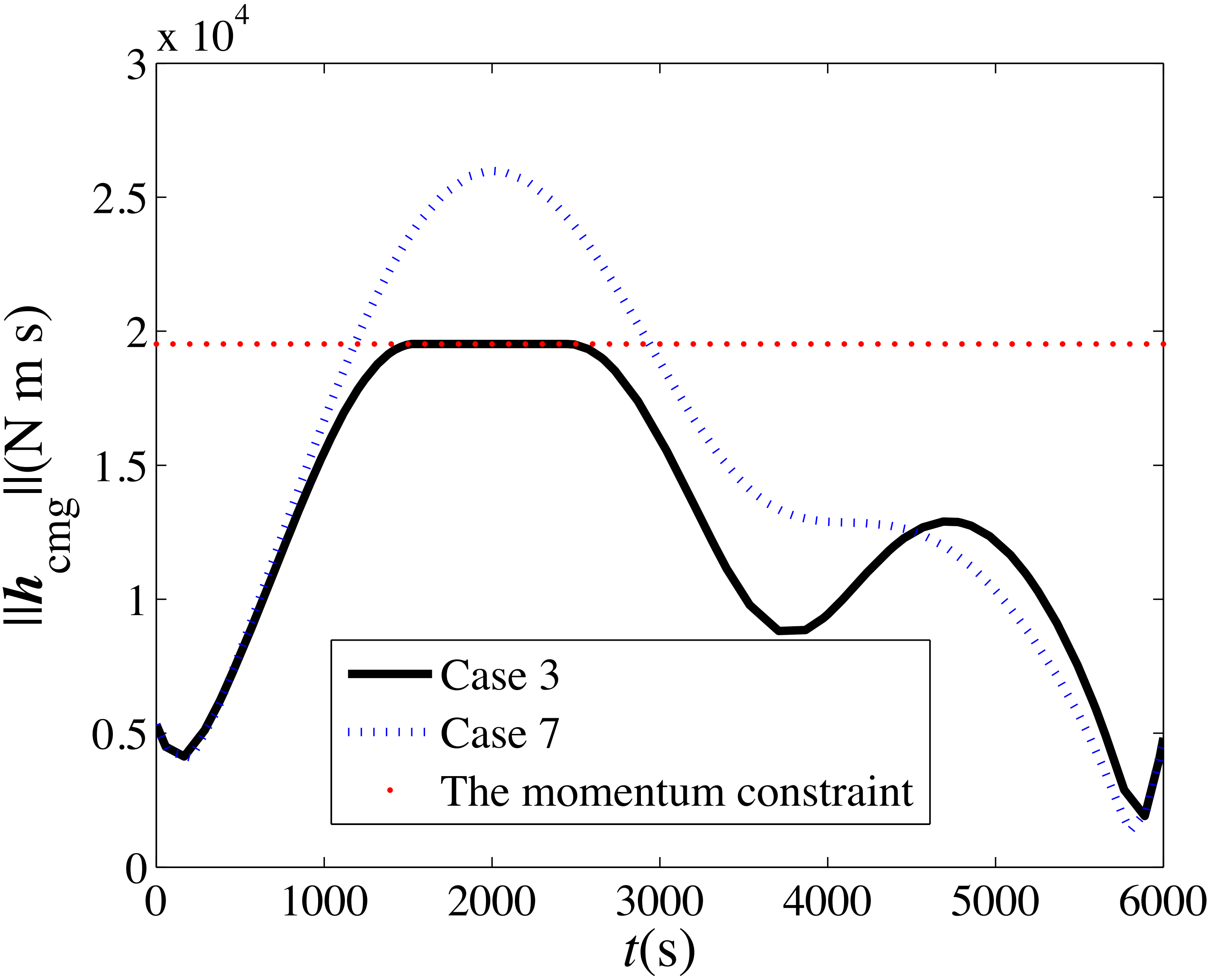

x 10^4
3
2.5
2
1.5
1
0.5
0
0
1000
2000
3000
4000
5000
6000
t(s)
||h_cmg||(N m s)
Case 3
Case 7
The momentum constraint

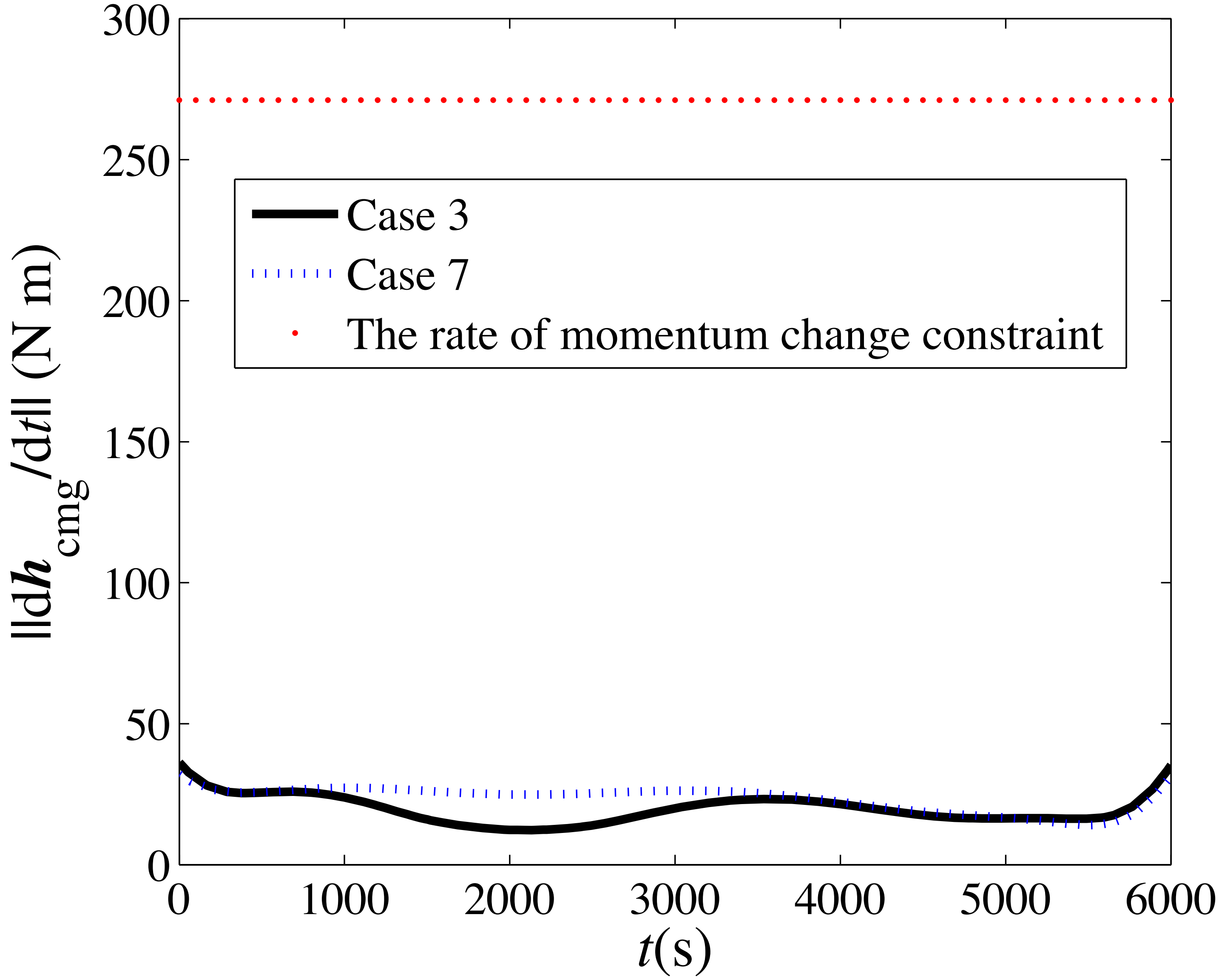

300
250
200
150
100
50
0
0
1000
2000
3000
4000
5000
6000
$\|\mathrm{d}\boldsymbol{h}_{\mathrm{cmg}}/\mathrm{d}t\|$ (N m)
t(s)
Case 3
Case 7
The rate of momentum change constraint

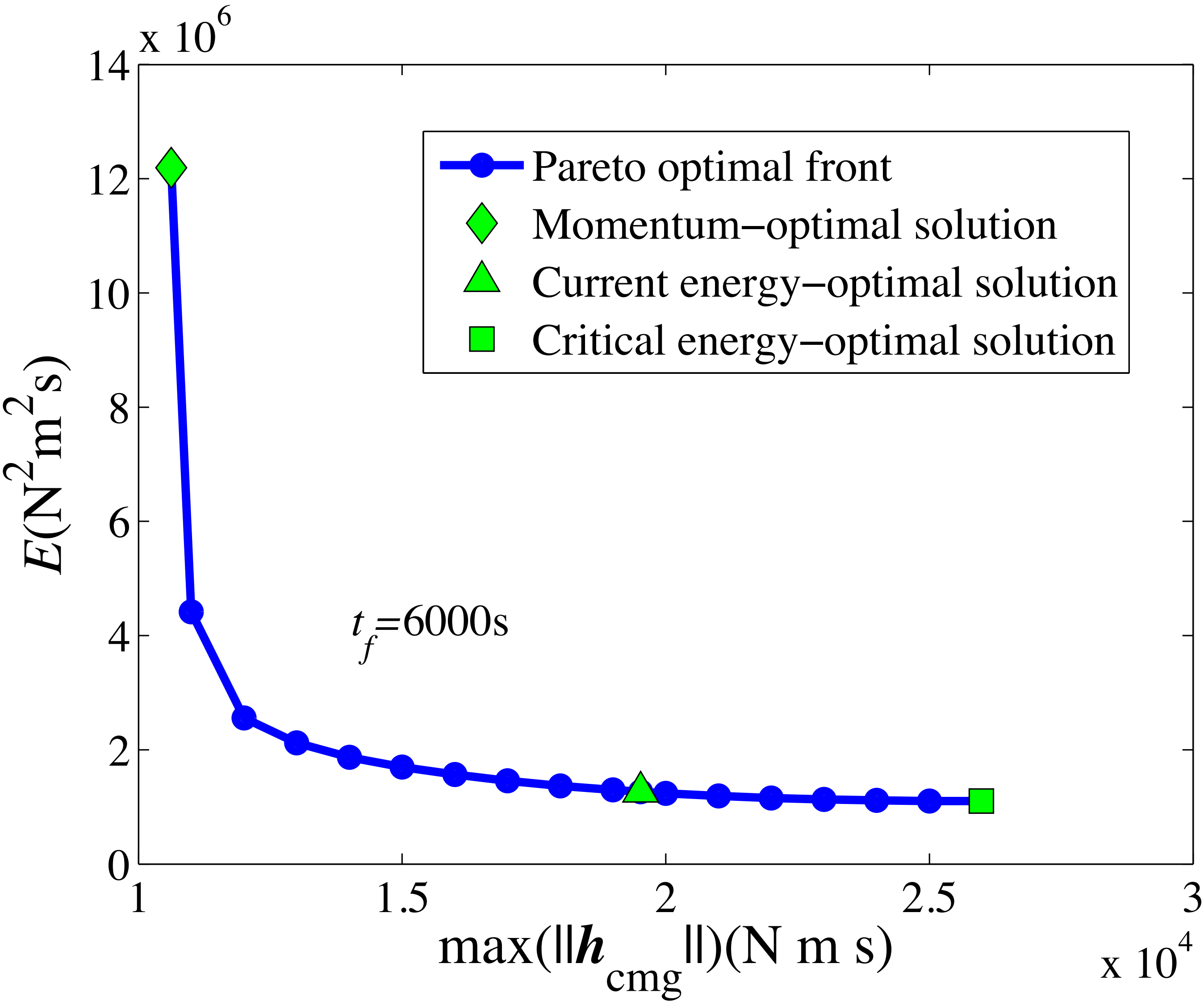

x 10^6
14
12
10
8
6
4
2
0
E(N^2m^2s)
Pareto optimal front
Momentum−optimal solution
Current energy−optimal solution
Critical energy−optimal solution
t_f=6000s
1
1.5
2
2.5
3
max(||h_cmg||)(N m s)
x 10^4

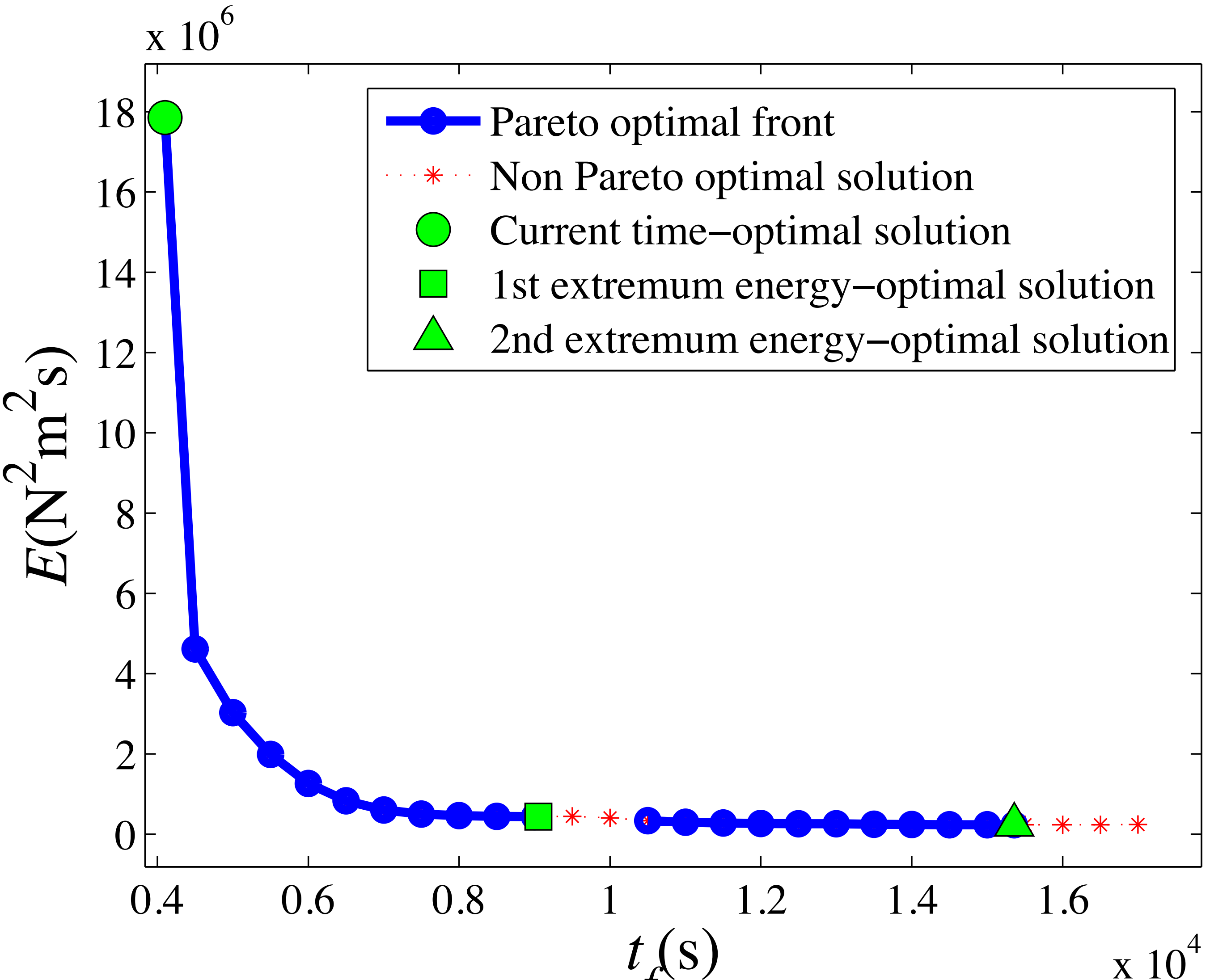

x 10^6
18
16
14
12
10
8
6
4
2
0
E(N^2m^2s)
0.4
0.6
0.8
1
1.2
1.4
1.6
t_f(s)
x 10^4
Pareto optimal front
Non Pareto optimal solution
Current time−optimal solution
1st extremum energy−optimal solution
2nd extremum energy−optimal solution

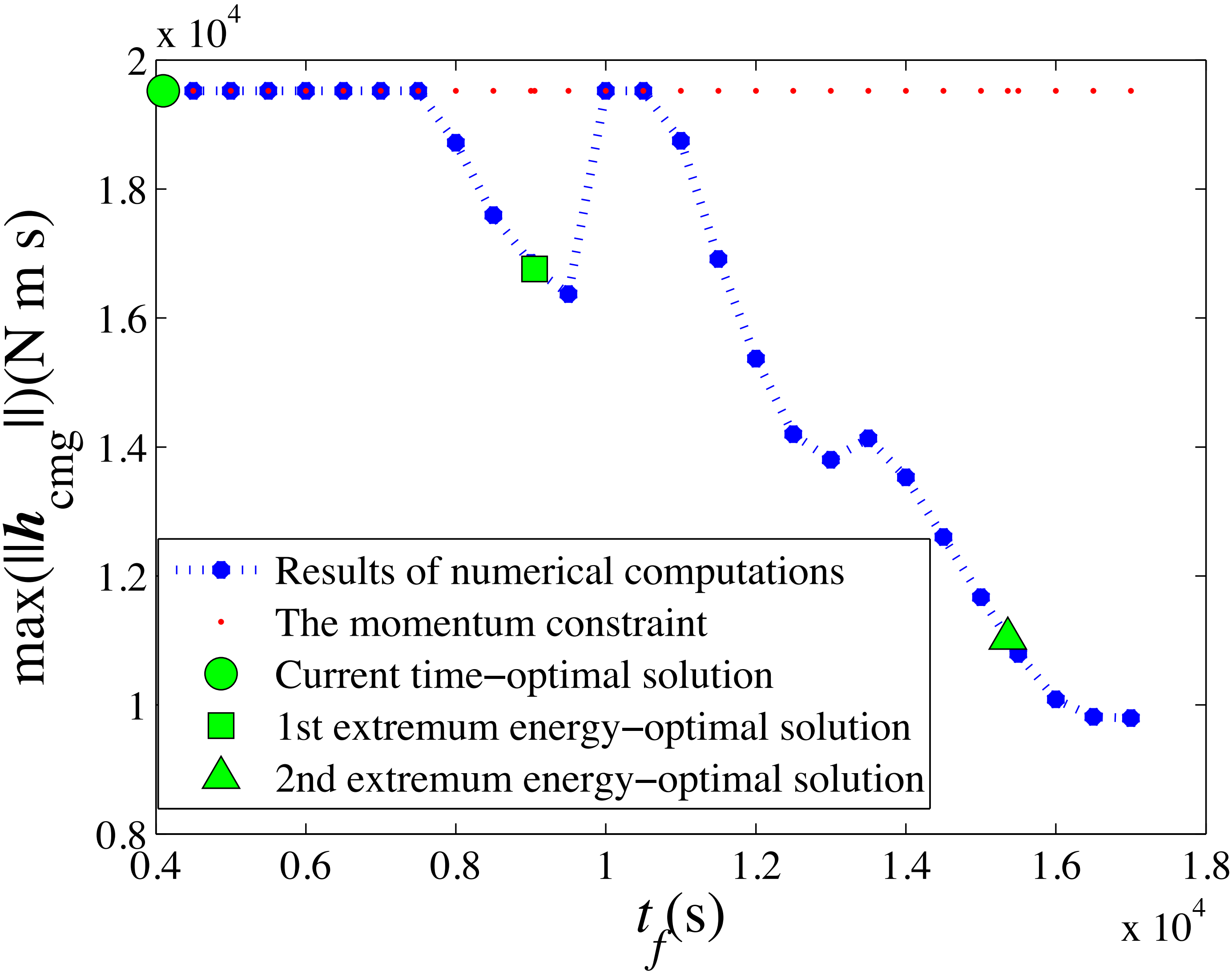

x 10^4
2
1.8
1.6
1.4
1.2
1
0.8
max(||h_cmg||)(N m s)
0.4
0.6
0.8
1
1.2
1.4
1.6
1.8
t_f(s)
x 10^4
Results of numerical computations
The momentum constraint
Current time−optimal solution
1st extremum energy−optimal solution
2nd extremum energy−optimal solution

Click here to download high resolution image

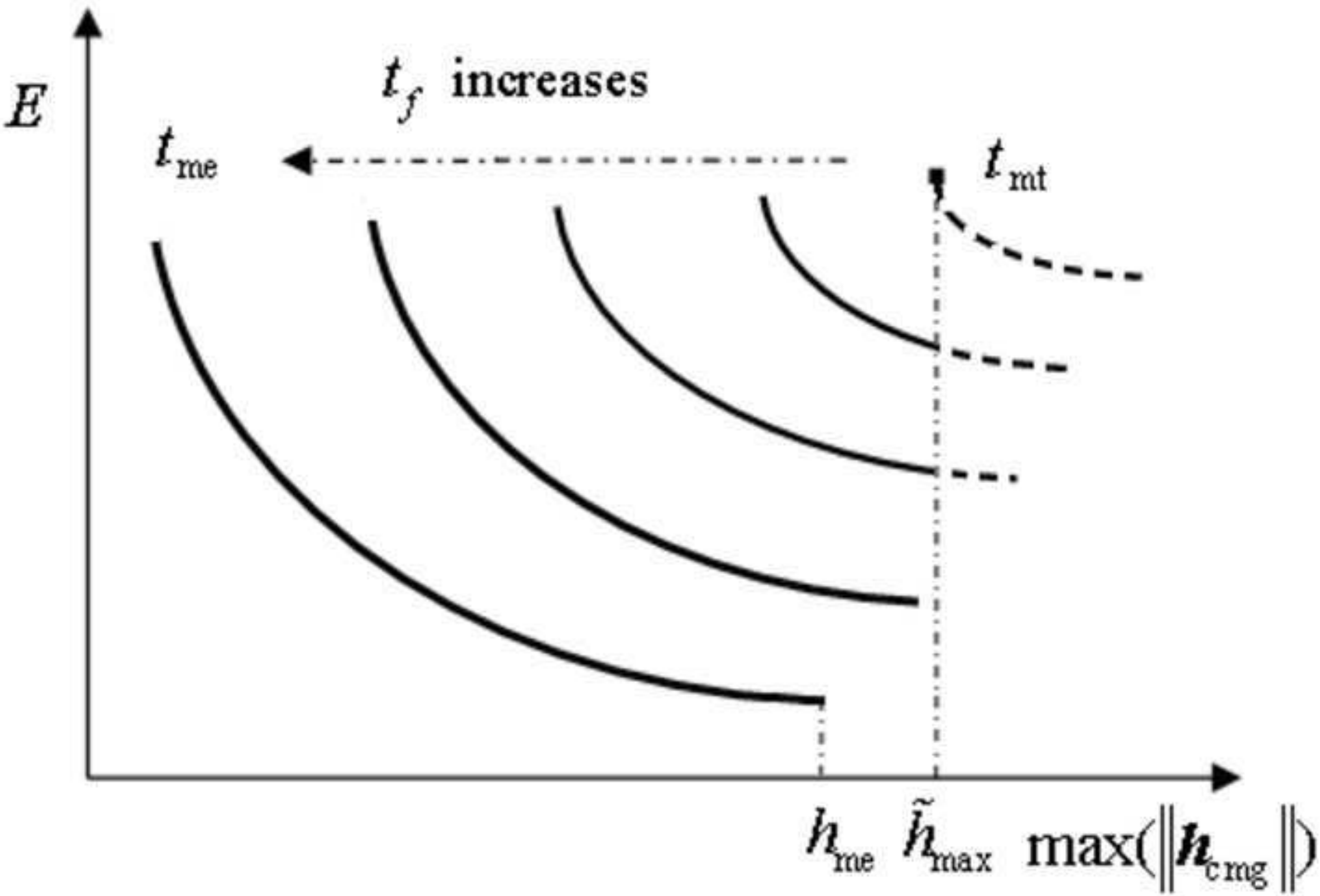

Click here to download high resolution image